Journal of Hydrology: Regional Studies 59 (2025) 102453

Contents lists available at ScienceDirect

Journal of Hydrology: Regional Studies

journal homepage: www.elsevier.com/locate/ejrh

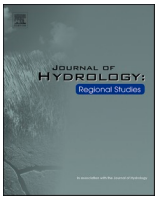

Assessing hydroclimatic impacts of climate change in snowy catchments using a physically based hydrological model

Frédéric Talbot [a,*], Jean-Daniel Sylvain [b], Guillaume Drolet [b], Annie Poulin [a], Jean-Luc Martel [a], Richard Arsenault [a]

[a] Hydrology, Climate and Climate Change Laboratory, École de technologie supérieure, Université du Québec, Montréal H3C 1K3, Canada
[b] Direction de la recherche forestière, Ministère des Ressources naturelles et des Forêts, Québec G1P 3W8, Canada

ARTICLE INFO

Keywords:
Hydrological modeling
Climate change impacts
Snowy catchments
Water balance Simulation Model

ABSTRACT

Study Region: This study focuses on 34 snowy catchments in Southern Quebec, Canada, characterized by diverse physiographic and hydrometeorological conditions. The region is particularly vulnerable to climate change due to its cold, snow-dominated hydrology and significant seasonal variability in temperature and precipitation.
Study Focus: The study evaluates future hydroclimatic changes using the Water flow and balance Simulation Model (WaSiM), a physically based distributed hydrological model. Hydroclimatic variables, including precipitation, snow water equivalent (SWE), streamflow, evapotranspiration, soil moisture, and groundwater recharge, were analyzed for reference (1981–2010) and future (2070–2099) periods.
New Hydrological Insights for the Region: The findings reveal significant shifts from snowfall to rainfall, reduced snow accumulation, and earlier snowmelt, leading to altered seasonal streamflow patterns, increased winter low flows, and earlier peak flows. Groundwater recharge and evapotranspiration are projected to rise during colder months, while surface runoff is expected to decline. In addition to analyzing individual variables, the study highlights how climate change alters the relationships between key hydrological processes, such as those linking groundwater recharge, soil moisture and evapotranspiration. These interdependencies underscore the importance of adopting a holistic approach to assess climate change impacts on the water cycle.

1. Introduction

The Earth's climate system is undergoing rapid changes, primarily driven by human-induced greenhouse gas emissions (Calvin et al., 2023; Yue and Gao, 2018). These changes have far-reaching implications for hydrological processes, altering water availability and quality (Gleick, 1989). Understanding the impacts of climate change on hydrology is crucial for effective water resources management and planning in the face of evolving climatic conditions (Milly et al., 2005; Sivakumar, 2011).

Boreal regions are particularly susceptible to climate change, experiencing rapid shifts in temperature and precipitation patterns, changing the duration of snow cover. Because they are located at higher latitudes, boreal regions are poised to see higher levels of warming compared to the world average (Estrada et al., 2021). Several studies have explored the potential impacts of climate change on hydrology, providing valuable insights into future water resources management. These investigations have projected changes such

* Corresponding author.
E-mail address: frederic.talbot.2@ens.etsmtl.ca (F. Talbot).

https://doi.org/10.1016/j.ejrh.2025.102453
Received 12 December 2024; Received in revised form 2 May 2025; Accepted 5 May 2025
Available online 14 May 2025

as altered streamflow regimes (Cochand et al., 2019; Gombault et al., 2015; Minville et al., 2008; Riboust and Brissette, 2015; Aygün et al., 2020a; Valencia Giraldo et al., 2023), delayed and shortened snow accumulation and melt periods (Novotná et al., 2013; Mudryk et al., 2018; Cochand et al., 2019; Aygün et al., 2020a; Nolin et al., 2023; Valencia Giraldo et al., 2023), changes in soil moisture and groundwater recharge annual patterns (Cochand, 2014; Dubois et al., 2022; Houle et al., 2012; Sulis et al., 2011), and shifts in the dominant hydrological processes (Gombault et al., 2015; Middelkoop et al., 2001; Novotná et al., 2013; Valencia Giraldo et al., 2023).

While these studies offer valuable insights into the potential impact of climate change on regional hydrology, they also face limitations in accurately projecting these changes under future conditions. Firstly, many investigations relied on the Coupled Model Intercomparison Project Phase 5 (CMIP5) models (Taylor et al., 2012), which have since been succeeded by the more advanced Model Intercomparison Project Phase 6 (CMIP6) models (O'Neill et al., 2016). Martel et al. (2022) demonstrated that climate change impact studies using CMIP5 should be repeated with CMIP6 models due to the improvements in processes representation in the new models. Secondly, the spatial scale of hydrological models used in most of these studies has often been lumped or distributed but conceptual in nature, limiting their ability to capture local heterogeneity and finer-scale processes (Han et al., 2021; McDonnell et al., 2021).

Accurate representation of processes within hydrological models is vital when evaluating climate change impacts (Kour et al., 2016; Talbot et al., 2024a). Conceptual models, which simplify complex hydrological processes, often assume parameter stationarity, which may not hold true under changing climatic conditions (Coron et al., 2014; Duethmann et al., 2020; Milly et al., 2008). Consequently, adopting physically based models can enhance the representation and robustness of hydrological processes, thereby improving our ability to assess future hydrological responses to climate change (Devia et al., 2015; Jones et al., 2006; Ludwig et al., 2009; Poulin et al., 2011; Wilby, 2005).

Recent research has employed advanced models and novel approaches to assess climate change impacts on hydrology, particularly in regions characterized by snowy conditions. One such model is the grid-based Water flow and balance Simulation Model (WaSiM) (Schulla, 2021), which has been effectively used to study hydrological responses to climate change across various regions. For instance, Gädeke et al. (2014) explored uncertainties in hydrological responses in Germany's Spree River catchment, finding significant variability due to different downscaling approaches. Bormann and Elfert (2010) evaluated the impacts of land use changes in Northern Germany, noting that WaSiM performed better in sloped and heterogeneous catchments. Additionally, Jasper et al. (2006) investigated changes in soil moisture in Switzerland's Thur river basin, demonstrating WaSiM's capability in capturing soil moisture dynamics under changing climatic conditions. In Scotland's Tarland catchment, Iacob et al. (2017) analyzed flood management strategies, showing how land use changes could mitigate flood risks, further highlighting WaSiM's versatility.

In Quebec, Canada, WaSiM has been applied to study the hydrological impacts of climate change. Novotná et al. (2013) examined water quality in an agricultural watershed, observing increased discharge and related water quality issues. Valencia Giraldo et al. (2023) used a refined neutral approach to assess the potential hydrological impacts of climate change in Quebec, revealing significant changes in annual water balances, snow reduction, and differential impacts on low flows. Ricard et al. (2019) explored an alternative framework of the hydroclimatic modeling chain using asynchronous objective functions to evaluate the effects of climate change on streamflow distribution. While these studies have made significant contributions to hydrological modeling, they also have certain limitations. For instance, they did not incorporate the latest advancements in climate modeling, such as the use of CMIP6 models, which could provide more accurate representations of future climate conditions. Additionally, these studies did not utilize the WaSiM groundwater module, which is essential for a comprehensive understanding of hydrological processes.

Physically based models such as WaSiM offer a powerful framework for assessing the impacts of climate change on hydrology, as they account for local heterogeneity and fine-scale processes. This capability is especially valuable in regions like Quebec, where hydrological dynamics are shaped by complex interactions among temperature, precipitation, and snow cover. In this study, we applied a multi-variable calibration of WaSiM to evaluate changes across key hydrological variables including rainfall, snowfall, snow water equivalent, evapotranspiration, soil moisture, surface runoff, and groundwater recharge. The analysis covers 34 catchments across Quebec, spanning approximately 54,000 square kilometers at a spatial resolution of 250 m. This high-resolution and large-scale assessment provides a rare and detailed view of how climate change influences both individual processes and the overall functioning of the water cycle. To our knowledge, while most climate change impact studies using spatially distributed models at high resolution focus on one or a few catchments (e.g., Gädeke et al., 2014; Bormann and Elfert, 2010; Jasper et al., 2006; Iacob et al., 2017; Novotná et al., 2013; Valencia Giraldo et al., 2023; Ricard et al., 2019), this work represents one of the most spatially extensive and finely resolved applications of WaSiM to date. Furthermore, unlike studies that primarily examine streamflow or a limited set of variables, our approach emphasizes the interconnected nature of hydrological processes and how these relationships evolve under future climate conditions. By covering a broad range of physiographic and climatic contexts, the study enhances the relevance and applicability of its findings for guiding adaptive water resource management in cold and snowy environments. Additionally, the methodologies and insights gained from this study have broader applicability to other regions with similar climatic and hydrological conditions, such as parts of Europe, North America, and Asia, thereby expanding the scope and relevance of the findings.

2. Materials and methods

2.1. Study area

The data and methods employed in this study, including study area selection, physiographic data, streamflow measurements, digital elevation model processing, land cover classification, soil type determination, and meteorological data interpolation, are consistent with those detailed in Talbot et al. (2024a). Readers are encouraged to refer to that publication for comprehensive information on data sources, processing techniques, and methodological approaches. A summary is presented in supplementary material.

The study focuses on 34 catchments located in Southern Quebec, Canada, selected for their diverse physiographic and hydrometeorological characteristics. These catchments, which range in area from 525 km^2 to 6840 km^2 (Fig. 1), are key components of the Hydroclimatic Atlas of Southern Québec (2022).

The Köppen climate classification for this region is primarily Dfb (Humid continental mild summer, wet all year), with some areas classified as Dfc (Subarctic with cool summers and year-round precipitation) (Beck et al., 2018). The region experiences significant seasonal climate variability (Fig. 2). During the winter months, which typically span from December to February, temperatures drop significantly, leading to prolonged freezing conditions. Snowfall is prevalent during this period, contributing to a substantial snowpack that persists throughout much of the season. The spring freshet typically begins between March and June, depending on the catchment location and local temperatures, as rising temperatures and increasing solar radiation trigger snowmelt and seasonal high flows.

Summer, from June to August, is characterized by warm temperatures and increased evapotranspiration. Average summer temperatures range from 15°C to 20°C. Rainfall remains relatively high during this period, which sustains streamflow despite higher evapotranspiration rates. However, evapotranspiration in these catchments is primarily energy-limited, meaning that available energy, rather than water supply, is the main constraint on evaporation and transpiration processes.

Fall, spanning from September to November, marks the transition from warm summer conditions to the onset of winter. Temperatures gradually decrease, and precipitation shifts toward a mix of rain and snow, particularly in higher elevations and northern catchments.

Key characteristics of the catchments, including area, mean elevation, annual total precipitation, annual extreme daily temperature, and annual streamflow, are summarized in Table 1.

Selected catchments remain mostly unaffected by the presence of dams and reservoirs, preserving the natural integrity of hydrological processes.

The study area encompasses various soil types and land covers. According to Sylvain et al. (2021), sandy loam is the predominant soil texture, constituting 72 % of the study area, while loam and loamy sand also feature prominently at 12 % and 11 %, respectively. Land cover patterns reveal that mixed forests cover 38 % of the study area, with coniferous and deciduous forests also each accounting for 23 % and 22 %, respectively. Crops and water are the only other significant land cover classes, at 6 % and 5 % respectively (Commission for Environmental Cooperation, 2020; Latifovic et al., 2012).

2.2. Data

2.2.1. Streamflow

This study utilized streamflow data from 1981 to 2010 from the Hydroclimatic Atlas of Southern Québec (2022). It is provided at the daily timestep and contains some minor periods of missing data. These include winter periods where flows can be affected by ice cover and ice jams and are therefore heavily biased, explaining their removal from the dataset. Most rivers are natural and unregulated. However, some have small weirs that control upstream sections of the watersheds. The resulting flows are considered

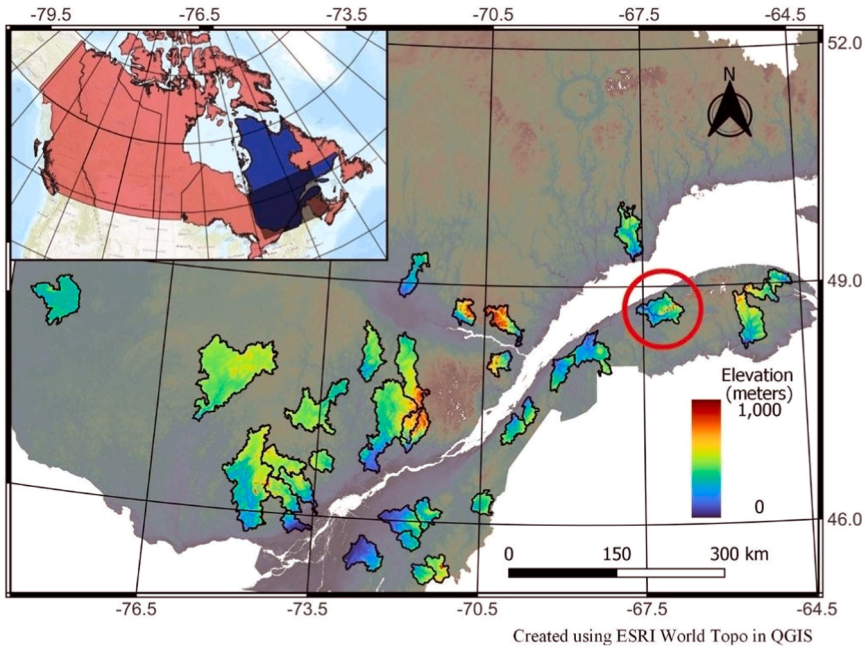

Fig. 1. Map showing the location of the 34 study catchments within Southern Quebec, Canada. The catchments are highlighted in various colors representing elevation. The catchment circled in red will be assessed in more details in this study. The inset provides the location of the province of Quebec in Canada.

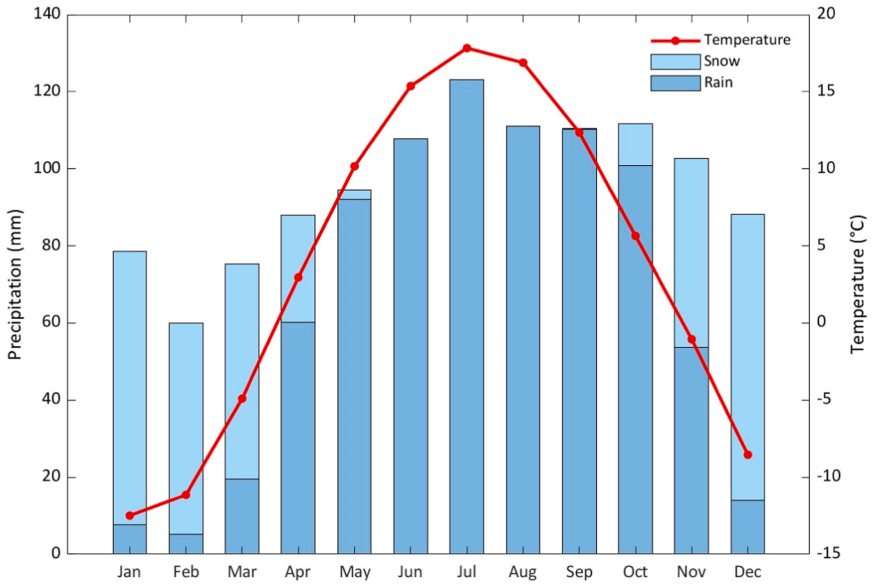

Fig. 2. Monthly average temperature (°C) and total precipitation (mm) for the study area, averaged over the 34 selected catchments. The red line represents the temperature trend, while the vertical bars indicate total precipitation, which is divided into the proportion falling as rain (dark blue) and snow (light blue), highlighting the seasonal variability and distinct four-season climate typical of Southern Quebec.

Table 1
Summary characteristics of key attributes for the 34 selected catchments during the period 1995–2009.

Catchment Characteristics	Minimum	Median	Maximum
Area (km^2)	525	1185	6840
Mean Elevation (m)	137	365	568
Annual Total Precipitation (mm)	933	1140	1395
Annual Minimum Daily Temperature (°C)	−37.7	−32.4	−27.8
Annual Maximum Daily Temperature (°C)	23.1	26.8	28.6
Annual Streamflow ($mm{\cdot}y^{-1}$)	461	629	996

unregulated despite these small deviations.

2.2.2. *Digital elevation model*

The digital elevation model (DEM) was derived from the NASA Shuttle Radar Topography Mission Global 1 arc second (SRTMGL1) version 3.0. Hydrological corrections based on provincial data ensured the accurate representation of hydrological networks, with adjustments made using SAGA GIS software (Conrad et al., 2015). Tanalys software (Schulla, 2021) was used to extract essential information, including slope, aspect, flow times, and river characteristics, for integration into the WaSiM hydrological model.

2.2.3. *Land cover*

Land cover data were sourced from the 2015 North American Land Change Monitoring System (NALCMS) 30 m dataset (Commission for Environmental Cooperation, 2020; Latifovic et al., 2012) and resampled using the nearest neighbor method at a 250 m resolution. Land cover can have a significant impact on hydrological parameters like root distribution, vegetation cover fraction (VCF), roughness length (Z0), and albedo which, in WaSiM, control processes such as evapotranspiration, runoff, and infiltration.

2.2.4. *Soil type*

To account for the spatial variability of soil hydraulic properties across the study area, we utilized the SIIGSOL 100 m database (Sylvain et al., 2021). The SIIGSOL database provides detailed descriptions of the proportions of sand, clay, and silt within the soil profile (Ministère des Ressources Naturelles et des Forêts, 2022). Soil type information was converted to soil texture classes based on the United States Department of Agriculture (USDA) classification system (Weil and Brady, 2017). Soil hydraulic properties were imputed from established relationships between soil texture classes and hydraulic parameters. SRTM elevation data was used to account for soil depth spatial variability. Higher elevations were assumed to have thinner soil thickness, while lower elevations were considered to have thicker soil. Raster cells with elevations below the 33rd percentile were classified as deep, those above the 66th percentile as shallow, and the remaining as normal.

2.2.5. Meteorological data

This study employed meteorological data from the ECMWF Reanalysis v5 (ERA5) dataset (Hersbach et al., 2020), which is known for its ability to mitigate the shortcomings of observational datasets and has demonstrated its effectiveness in this region (Tarek et al., 2020). We chose ERA5 due to its comprehensive coverage and reliability, particularly in regions where observational data may be sparse or inconsistent. Specifically, we focused on total precipitation and mean temperature, using daily temporal resolution, for a period spanning from 1981 to 2020. Meteorological data were further interpolated for each watershed at the 250 m spatial resolution used by the model. The interpolation was run directly in WaSiM using the inverse distance weighting (IDW) method as recommended by Schulla (2021).

2.2.6. Climate projections

As suggested by Martel et al. (2022), who conducted a North America-wide comparison of CMIP5 and CMIP6 climate and hydrological projections across over 3000 catchments including our study area, we used projected daily temperature and precipitation data from CMIP6 models (O'Neill et al., 2016) for both the reference (1981–2010) and future (2070–2099) periods. According to Martel et al., CMIP6 projections generally indicate warmer and wetter futures, with reduced inter-model spread for both temperature and precipitation, thereby increasing confidence in the assessment of future hydroclimatic changes. To address and assess the uncertainty related to the selection of climate models (Arsenault et al., 2020; Lucas-Picher et al., 2021; Minville et al., 2008; Tarek et al., 2021), an ensemble of 18 climate models was employed, as shown in Table 2.

The multivariate bias correction algorithm (MBCn) (Cannon, 2018) was utilized to correct biases in the climate model simulations. While MBCn was not independently validated in our study region, its effectiveness has been well documented in the literature. Guo et al. (2020) and Dieng et al. (2022) both demonstrated that MBCn significantly improves climate model outputs by reducing biases and preserving inter-variable dependencies across a range of hydroclimatic contexts. This method allows to correct biases in meteorological data, while accounting for spatiotemporal interdependencies between variables and preserving changes in quantiles between the reference and future periods. This was performed on daily total precipitation and mean temperature using the ERA5 data as the reference data over the period 1981–2010, then applying the transformation to the climate models data over the reference (1981–2010) and future (2070–2099) periods.

This study utilized climate simulations from the Shared Socioeconomic Pathway 5–8.5 (SSP5–8.5), a scenario projecting very high greenhouse gas emissions with global warming exceeding 4 degrees Celsius by 2100 (Calvin et al., 2023). While some authors argue that these "hot" models are unrealistic, this remains a subject of much debate in the scientific community (Calvin et al., 2023; Hausfather et al., 2022). In this study, the SSP5–8.5 models were used to provide a picture of the future climate of the region under the worst plausible conditions. Fig. 3 shows a consistent increase in future monthly precipitation throughout the year across the catchments and models, especially from November to April. Additionally, temperatures are projected to rise significantly, with an increase of 5–8 degrees Celsius, consistent with IPCC projections. This trend aligns with expectations for northern latitudes, which are anticipated to warm faster than the global average (Estrada et al., 2021). Fig. 4 presents the spatial distribution of annual mean

Table 2
Global climate models (GCMs) used in the study and their associated institutions.

ID	GCM	Source	Institution
CM1	ACCESS-ESM1–5	(Ziehn et al., 2020)	Australian Community Climate and Earth System Simulator, Australia
CM2	CMCC-ESM2	(Lovato et al., 2022)	Centro Euro-Mediterraneo sui Cambiamenti Climatici, Italy
CM3	CanESM5	(Swart et al., 2019)	Canadian Centre for Climate Modelling and Analysis, Canada
CM4	EC-Earth3	(Döscher et al., 2022)	European consortium of national meteorological services and research institutes; Spain, Denmark, Italy, Finland, Germany, Ireland, Portugal, Netherlands, Sweden, Norway, and Belgium.
CM5	EC-Earth3-CC		
CM6	EC-Earth3-Veg-LR		
CM7	FGOALS-g3	(Pu et al., 2020)	Chinese Academy of Sciences, China
CM8	GFDL-ESM4	(Krasting et al., 2018)	Geophysical Fluid Dynamics Laboratory, USA
CM9	INM-CM4–8	(Volodin et al., 2019)	Institute for Numerical Mathematics, Russia
CM10	INM-CM5–0		
CM11	IPSL-CM6A-LR	(Boucher et al., 2020)	Institut Pierre Simon Laplace, France
CM12	MIROC6	(Tatebe et al., 2019)	Japan Agency for Marine-Earth Science and Technology, Japan
CM13	MPI-ESM1–2-HR	(Mauritsen et al., 2019)	Max Planck Institute for Meteorology, Germany
CM14	MPI-ESM1–2-LR		
CM15	MRI-ESM2–0	(Yukimoto et al., 2019)	Meteorological Research Institute, Japan
CM16	NESM3	(Cao et al., 2021)	Nanjing University of Information Science and Technology, China
CM17	NorESM2-LM	(Seland et al., 2020)	Norwegian Climate Centre, Norway
CM18	NorESM2-MM		

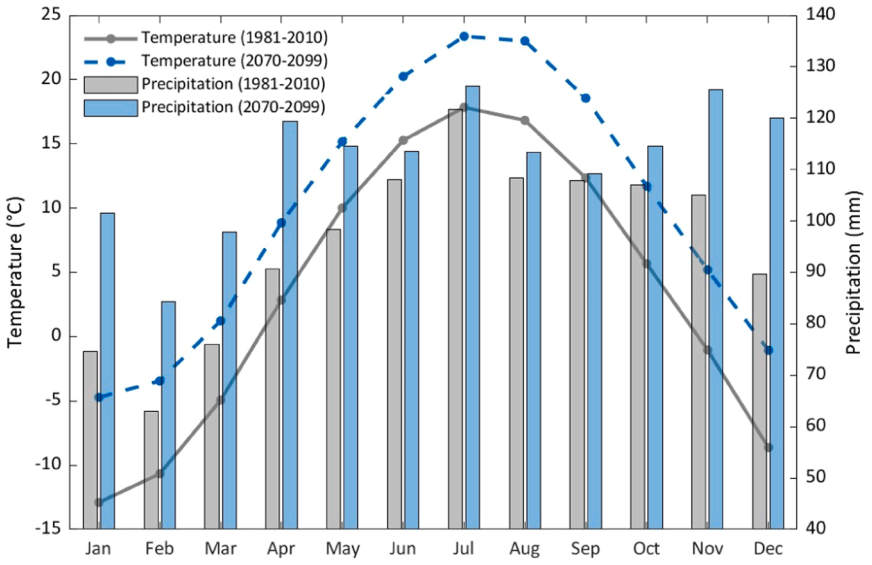

Fig. 3. Monthly total precipitation and mean temperature for the reference (1981–2010) and future (2070–2099) periods under the Shared Socioeconomic Pathway 5–8.5 (SSP585) scenario after bias-correction for the study area, averaged over the selected catchments and 18 climate models used in the study. The solid lines represent the average monthly mean temperature for the reference (grey) and future (blue dashed line) periods, while the vertical bars indicate the average monthly total precipitation for the reference (grey) and future (blue) periods.

temperatures and annual total precipitation for the reference period as well as projected changes for the future period.

2.3. WaSiM model

In this study, the WaSiM version 10.06.00 was utilized for hydrological modeling (Schulla, 2021). WaSiM allow to accurately model key hydrological processes in three dimension through a deterministic and spatially distributed approach (Ricard et al., 2020). However, WaSiM's complexity involves the necessity for high-quality input data, which can be seen as a limitation of this model due to

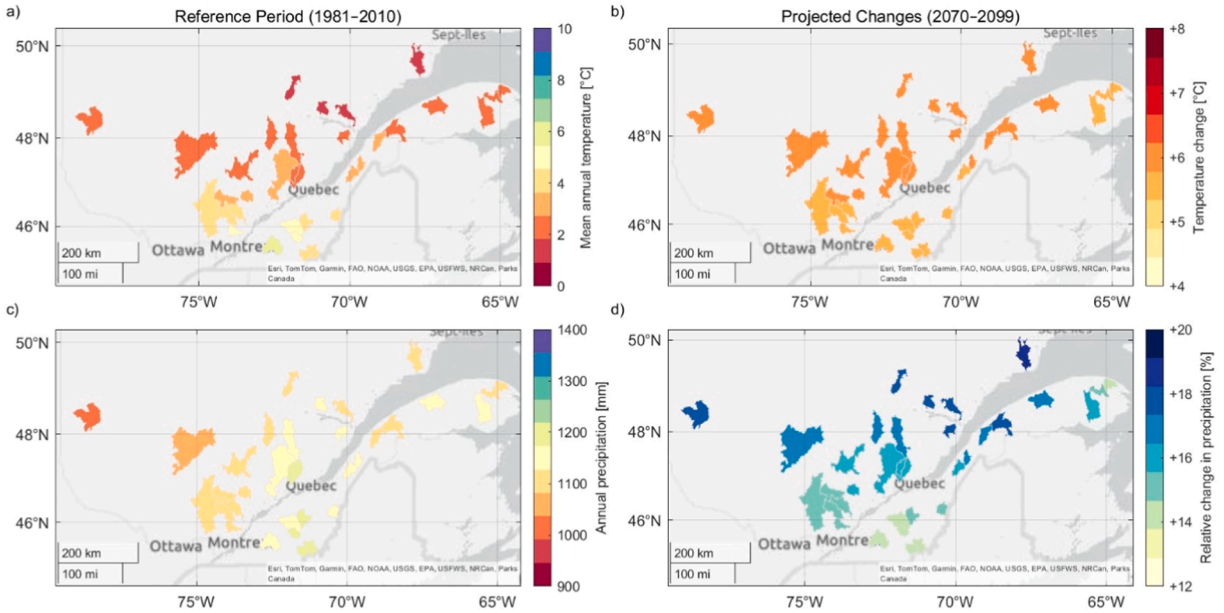

Fig. 4. Spatial distribution of mean annual temperature (°C) and annual precipitation (mm) across selected catchments: Panel (a) depicts the reference period (1981–2010) for temperature, while Panel (b) shows projected changes (2070–2099) under the SSP5–8.5 scenario. Panel (c) displays reference-period precipitation, and Panel (d) illustrates projected changes (%) for the same future period and scenario. Data in panels (a) to (d) are averages from the 18 climate models used in this study.

potential data uncertainties and increased computational demands (Beven, 2001; Blöschl and Sivapalan, 1995).

WaSiM is available in two versions: one using the Topmodel approach and another using the Richards equation (Richards, 1931). We selected the Richards equation version for its physically based simulation of hydraulic head gradients and the integration of soil properties. This version allows for a more detailed and realistic representation of infiltration and subsurface processes, which is particularly important for the diverse physiographic and soil conditions across the study catchments. Additionally, the Topmodel version has been discontinued in newer versions of WaSiM, further supporting the use of the Richards equation approach in this study. Based on research needs, WaSiM allows the activation of specific sub-models, which can be parallelized to optimize efficiency and reduce computational demands.

The configuration used for this study included activating the groundwater flow sub-model using the Gauss-Seidel iteration method and employing the Hamon method for the evapotranspiration sub-model. The remainder of the model configuration mirrors that described in Talbot et al. (2024a).

2.4. Model calibration

2.4.1. Calibration parameters

The calibration process involved fine-tuning 17 parameters (Table 3), selected based on the recommendations provided in the WaSiM documentation (Schulla, 2021). The rest of the parameters in the control file were kept at their default values as specified in the documentation. This calibration approach mirrors configuration GW-RC described in Talbot et al. (2024a). Table 3 was taken from Talbot et al. (2024a).

2.4.2. Calibration framework

For model calibration, the study employed split-sample test (SST) framework. This widely used approach involves dividing the available streamflow data into two sets: one for calibrating the model and the other for validating its performance. This method is particularly useful in hydrology for testing a model's ability to generalize beyond the conditions under which it was calibrated, providing a measure of model's performance and reliability. The calibration period (2000–2009) was chosen based on the availability of reliable hydrological data, with specific adjustments for certain catchments (Croche: 1995–1999, Petit Saguenay: 1995–1999, and Sainte-Marguerite Nord-Est: 1992–1996). Similarly, the validation period was set for 1990–1999, except for the Croche (1986–1994), Petit Saguenay (1986–1994), and Sainte-Marguerite Nord-Est (1986–1991) catchments. A five year spin-up period was performed before each simulation to allow the model to reach a stable state, limiting the effect of unstable initial conditions on the model's performance metrics (Ekmekcioğlu et al., 2022).

The optimization algorithm employed for the calibration process was the dynamically dimensioned search (DDS; (Tolson and Shoemaker, 2007)) algorithm, following the recommendation of Arsenault et al. (2014). This algorithm is specifically designed for efficiently calibrating complex hydrological models with a large parameter range given a finite computing budget. It dynamically adapts its search strategy based on the number of evaluations performed and converges accordingly.

The calibration process was divided into two main phases: pre-calibration and calibration. This sequential calibration is designed to refine the model's performance progressively. The strategy of starting with a wider parameter space and progressively narrowing it ensured a comprehensive and targeted calibration, ultimately enhancing the model's ability to simulate the hydrological dynamics of

Table 3
Parameter description and values used for calibrating WaSiM in each watershed.

No.	Code	Description	Unit	Sub-Model	Range
1	k_D	Storage coefficient for surface runoff	h	Unsaturated zone	[1,25]
2	k_H	Storage coefficient for interflow	h	Unsaturated zone	[1,25]
3	d_r	Drainage density for interflow	m^{-1}	Unsaturated zone	[1,50]
4	QD_{Snow}	Fraction of surface runoff on snow melt	-	Unsaturated zone	[0.1, 1]
5	c_0	Degree-Day factor	mm $°C^{-1}d^{-1}$	Snow	[0,3]
6	T_0	Temperature limit for snow melt	°C	Snow	[−4, 4]
7	$T_{R/S}$	Transition temperature snow/rain	°C	Snow	[−4, 4]
8	C_{WH}	Water storage capacity of snow	-	Snow	[0.1, 0.3]
9	C_{rfr}	Coefficient for refreezing	-	Snow	[0.1, 1]
10	$f_{i,summer}$	Summer correction factors for ETP	-	Evapotranspiration	[0.1, 2]
11	$f_{i,fall}$	Fall correction factors for ETP	-	Evapotranspiration	[0.1, 2]
12	$f_{i,winter}$	Winter correction factors for ETP	-	Evapotranspiration	[0.1, 2]
13	$f_{i,spring}$	Spring correction factors for ETP	-	Evapotranspiration	[0.1, 2]
14	K_{rec}	Recession constant for hydraulic conductivity	-	Soil table	[0.1, 0.99]
15	d_z^a	Soil layer thickness	-	Soil table	[0.8, 1.4]
16	Kol^b	Colmation of the river links	-	Input grid	[1100]
17	K_{XY}^c	Saturated horizontal conductivity	m s^{-1}	Input grid	[0.2, 4]

[a]Calibration coefficient, ranging from 0.8 to 1.4, is applied to adjust the total soil depth, which is predetermined to be 8 m for shallow, 14 m for normal, and 20 m for deep soil conditions.
[b]Calibration coefficient, ranging from 1 to 100, is applied to adjust the colmation grid, which is predetermined to be 1×10^{-6}.
[c]A calibration coefficient, ranging from 0.2 to 4, is applied to adjust the saturated horizontal conductivity grid, which is predetermined to be 4×10^{-5} m s^{-1}.

the catchments, which is critical for an application in climate change conditions.

A key aspect of this methodology is the inclusion of groundwater recharge in the calibration process, ensuring that both surface and subsurface hydrological processes are realistically represented. By integrating recharge constraints alongside streamflow, this approach mitigates equifinality issues and enhances the model's ability to simulate hydrological dynamics under changing climate conditions. This multi-variable calibration strategy, as highlighted in Talbot et al. (2024a), represents a key novelty of the study, as it improves the physical consistency of hydrological simulations, ultimately leading to more robust climate change impact assessments.

2.4.3. Pre-calibration

The pre-calibration involved defining parameter ranges for parameters that mostly impact baseflow (d_r, QD_{Snow}, K_{rec}, Kol, Kxy). The pre-calibration involved 200 evaluations using grids with a spatial resolution of 1000 m, followed by 50 evaluations using grids with a resolution of 250 m. This multi-resolution approach enhances computational efficiency while maintaining reasonable model performance. Preliminary tests showed that increasing the number of simulations beyond 50 at the finer scale provided negligible improvements, making further computational expense unnecessary. Similar strategies are commonly used in surrogate modeling to balance computational demand with model accuracy (Meert et al., 2018).

To ensure realistic groundwater recharge representation, the objective function used during pre-calibration included the Kling-Gupta Efficiency (KGE) (Kling et al., 2012) as the primary metric, supplemented by constraints on the mean (250 mm yr^{-1}) and standard deviation (80 mm yr^{-1}) of annual recharge (Eq. (3)). These recharge benchmarks were established based on regional studies (Buffin-Bélanger et al., 2015; Carrier et al., 2013; Cloutier et al., 2015, 2013; Comeau et al., 2013; Larocque et al., 2015, 2013; Lefebvre et al., 2015; Rouleau et al., 2013), and broadly reflect recharge conditions in the studied catchments. The inclusion of recharge constraints helps prevent parameter sets that produce acceptable streamflow simulations but unrealistic groundwater dynamics, addressing a key limitation in traditional streamflow-only calibrations (Talbot et al., 2024a)

Following the pre-calibration at both spatial resolutions, the resulting parameter sets were used to define new calibration ranges. Parameters values affecting baseflow (dr, QDSnow, Krec, Kol, Kxy) were adjusted in a range that maintain minimum and maximum values within ± 10 % of the optimal values obtained during pre-calibration. This ensures that recharge dynamics remain physically consistent while allowing some flexibility in parameter optimization. This two-steps calibration enhances the model's ability to simulate the full hydrological cycle, while maintaining groundwater recharge behaviour, making it more reliable for assessing climate change impacts on both surface and subsurface hydrological processes (Talbot et al., 2024a).

2.4.4. Calibration

The main calibration phase consisted of 1000 evaluations at a 1000-meter resolution, followed by 50 evaluations at a finer 250-meter resolution for final refinement. This phase was conducted using the adjusted parameter ranges from pre-calibration, employing a less restrictive objective function (Eq. (4)) to account for uncertainties in recharge estimates. The objective function primarily emphasized the Kling-Gupta Efficiency (KGE) (Kling et al., 2012), with a weighting of 4 % for the standard deviation of recharge. This weighting was selected based on preliminary tests, which evaluated different combinations on a test catchment and found that 96 % for KGE and 4 % for recharge standard deviation provided the best balance between optimizing streamflow performance and improving the overall representation of hydrological processes. Specifically, this approach helped prevent the model from relying excessively on interflow to match observed streamflow, thereby allowing for a more physically consistent partitioning between surface runoff, interflow, and groundwater recharge during spring melt (Talbot et al., 2024a).

Additionally, as the initial recharge estimate of 250 mm yr^{-1} was a broad regional estimate, this approach allowed the model to adjust recharge rates based on the specific hydrological and climatic characteristics of each catchment.

2.4.5. Performance metric

Calibration metrics were based on a weighted combination of the Kling-Gupta Efficiency (KGE) for streamflow, along with the mean and standard deviation of annual groundwater recharge. However, only the unweighted KGE for streamflow was used for model performance assessment and result interpretation, in order to maintain consistency for comparison across catchments and with other studies. The KGE (Eq. (1)) is a widely used hydrological metric that integrates correlation, variability, and bias, ranging from $-\infty$ to 1, with 1 indicating a perfect match between observed and simulated streamflow:

$$KGE = 1 - \sqrt{(r-1)^2 + \left(\frac{\mu_{sim}}{\mu_{obs}} - 1\right)^2 + \left(\frac{\frac{\sigma_{sim}}{\mu_{sim}}}{\frac{\sigma_{obs}}{\mu_{obs}}} - 1\right)^2}, \quad (1)$$

where r is the correlation coefficient, calculated as:

$$r = \frac{\sum_{i=1}^{n}(O_i - \overline{O}) * (S_i - \overline{S})}{\sqrt{\sum_{i=1}^{n}(O_i - \overline{O})^2 * \sum_{i=1}^{n}(S_i - \overline{S})^2}}, \quad (2)$$

here, O_i and S_i are the observed and simulated streamflow values for each day, respectively, and $\overline{O}$ and $\overline{S}$ are their respective means.

The weights used in the objective function for pre-calibration and calibration were determined through preliminary tests. These tests involved evaluating different weight combinations on a test catchment to find an optimal balance between achieving high KGE

and maintaining reasonable variability in groundwater recharge. The chosen weightings provided the best compromise, ensuring that the model performs well overall while accurately representing groundwater recharge dynamics.

The objective function used for the pre-calibration and calibration are defined in Eq. (3) and Eq. (4) respectively.

$$Objective\ function = 1 - \left(0.7 * KGE + 0.2 * \lceil \sigma_{r_{sim}} - 0.08 \rceil + 0.1 * \lceil \overline{r_{sim}} - 0.25 \rceil \right), \tag{3}$$

$$Objective\ function = 1 - \left(0.96 * KGE + 0.04 * \lceil \sigma_{r_{sim}} - 0.08 \rceil \right) \tag{4}$$

where $\sigma_{r_{sim}}$ represents the simulated annual recharge standard deviation (m yr^{-1}), $\overline{r_{sim}}$ is the simulated mean annual recharge (m yr^{-1}) and *KGE* is the Kling-Gupta efficiency.

2.5. Climate change assessment

2.5.1. Reference and future period simulations

For all catchments, simulations were performed using meteorological data from ERA5 for the reference period (1981–2010). Additionally, simulations were conducted using the 18 climate models from CMIP6 for both the reference period (1981–2010) and the future period (2070–2099). These simulations provided a comprehensive dataset to analyze historical conditions and project future changes.

2.5.2. Comparison of hydroclimatic variables

A regional comparative analysis was conducted on key hydroclimatic variables under reference and projected conditions and for ERA5 and CMIP6 data, including precipitation, snowfall, streamflow, surface runoff, interflow, actual evapotranspiration (ETa), baseflow, groundwater recharge, snow water equivalent (SWE), and soil moisture.

First, annual totals (annual means for soil moisture and annual maximums for SWE) of each variable were compared between ERA5 and CMIP6 simulations for the reference period. This comparison aimed to verify the adequacy of bias correction and the effectiveness of CMIP6 simulations in representing hydroclimatic variables for the reference period. Next, the relative changes between future and reference period simulations were calculated using the climate models outputs for both periods. The mean and standard deviation of these relative changes were computed across all catchments to quantify the overall impact of climate change on hydroclimatic variables across the study area and for the future period. Additionally, a comparative analysis of hydroclimatic variables was performed to validate the similarities between ERA5 and CMIP6 simulations for the reference period and to assess the differences between future and reference periods in terms of the timing and magnitude. Furthermore, the contributions of surface runoff, baseflow, interflow, and ETa to the water cycle were calculated for each climate model for both the reference and future periods. This analysis helped in understanding the potential redistribution of water within the hydrological cycle under future climate scenarios.

In addition to the regional analysis, particular emphasis was placed on the Matane catchment due to its representative hydrological characteristics. Specific comparisons of hydroclimatic variables were conducted at a finer scale for this catchment to provide a more granular understanding of climate change impacts. The Matane catchment analysis complements the broader regional assessment by offering insights into localized hydrological responses and variability.

2.5.3. Spatial representation of direction and magnitude of change

A spatial representation of the direction and magnitude of change for multiple hydroclimatic variables was performed using criteria from the Hydroclimatic Atlas of Southern Québec (2022), outlined in Table 4.

This classification allowed for a detailed spatial analysis, comparing the changes predicted by different climate models and identifying areas with consistent trends. The spatial analysis focused on hydrological indicators such as streamflow, groundwater recharge, and SWE, providing a clear visualization of regional impacts.

Table 4
Criteria for determining the direction of change in hydrological variables based on consensus among climate models indicating an increase or decrease.

Direction of Change	Criteria
Highly Probable Increase	More than 16 climate models indicate an increase.
Probable Increase	12–16 climate models indicate an increase.
No Consensus	7–11 climate models indicate an increase or decrease. The lack of consensus may indicate a weak change or widely dispersed climate models.
Probable Decrease	12–16 climate models indicate a decrease.
Highly Probable Decrease	More than 16 climate models indicate a decrease.

3. Results

3.1. Model calibration and validation

The model consistently achieved KGE scores above 0.5 across all catchments during both the calibration and validation phases.

During the calibration period, the minimum KGE achieved was 0.637 (Eaton), while the maximum was 0.877 (Matane), with a median value of 0.803. For the validation period, the minimum KGE was 0.661 (Eaton), the maximum was 0.869 (Bras du Nord), and the median value was 0.770. These results, including the similarity in KGE values between the calibration and validation periods, indicate an agreement between the observed and simulated streamflow data, supporting the model reliability for climate change assessment.

As for volume error, the mean volume error across catchments is −0.71 % ($\sigma = 2.79$) during the calibration period and 1.15 % ($\sigma = 5.02$) during the validation period. Most catchments fall within ± 5 % error in both periods. The largest discrepancies are observed for Eaton and de l'Achigan, with volume errors around 13 % during validation period (Table S2). Maintaining low volume errors is important to ensure that the model accurately represents the overall water balance, which is fundamental when analyzing long-term hydrological changes under future climate scenarios. This low level of error indicates that the model conserves mass effectively and provides a reliable representation of the overall water balance, which is essential when assessing the magnitude and direction of hydrological changes under future climate scenarios. The Eaton catchment exhibited the lowest model performance, with a KGE of 0.637 in calibration and 0.661 in validation, making it the only catchment with a calibration KGE below 0.71. The primary limitation in this catchment was the difficulty in accurately simulating winter flows, as the model exhibited an overly reactive response to snowmelt events. In this case, snowmelt was rapidly converted into surface runoff, leading to exaggerated flow peaks. This limitation is related to the WaSiM configuration used in this study. Additionally, the Eaton catchment has a higher proportion of cropland (27 %) compared to the average across all catchments (8 %). The presence of artificial drainage systems may further alter flow dynamics in ways that are not fully represented by the model, potentially contributing to the lower performance.

3.2. Regional hydrological changes

3.2.1. Comparative analysis of hydrological changes

This section presents a global overview of hydrological changes across the selected catchments. Table 5 provides a detailed comparison of various hydroclimatic variables simulated by WaSiM for the reference period (1981–2010), using ERA5 and CMIP6 data, and for the future period (2070–2099) using CMIP6 data only. It presents the mean relative changes, biases and standard deviations across the 34 catchments for each simulated variable, quantifying the impact of climate change on the water cycle. The standard deviation is calculated from the mean relative changes across the 34 catchments. The mean relative change for each catchment is obtained by averaging the relative changes from all climate models.

The similarity in averaged hydroclimatic variables between the ERA5 and CMIP6 simulations during the reference period indicates the consistency of the hydrological model and the effectiveness of the bias correction implementation.

Comparing the CMIP6 simulations between the reference and future periods reveals several significant differences. There is a notable shift in the ratio of snow to rain, with a 36 % increase in rain and a 33 % decrease in snow in the future period. Consequently, total precipitation rises from 1236 mm in the reference period to 1416 mm in the future, marking a 15 % increase.

Although the annual total streamflow remains similar between the reference and future periods, notable changes occur in the hydroclimatic variables. Surface runoff decreases by 34 %, while interflow, baseflow, and ETa increase by 24 %, 15 %, and 34 %, respectively. Groundwater recharge sees a 12 % increase, while snow SWE decreases by 47 % and soil moisture stays constant (0.21 %).

Fig. 5 presents the annual fluctuation of eight hydroclimatic variables over the reference and future periods for ERA5 and CMIP6 meteorological inputs. Again, the similarity between hydroclimatic variables resulting from simulations driven with ERA5 and CMIP6

Table 5
Comparison of hydroclimatic variables for reference and future periods across all catchments.

Hydroclimatic Variables	Unit	Reference (1981–2010)			Future (2070–2099)		
		ERA5	*CMIP6*	*Relative Bias (%)*	*CMIP6*	Relative change	
						Mean	*Std.*
Precipitation	$mm{\cdot}y^{-1}$	1248	1236	−0.98 %	1416	15 %	4 %
Rainfall	$mm{\cdot}y^{-1}$	859	850	−1.04 %	1156	36 %	5 %
Snowfall	$mm{\cdot}y^{-1}$	389	386	−0.83 %	260	−33 %	7 %
Streamflow	$mm{\cdot}y^{-1}$	661	652	−1.39 %	656	0.51 %	4 %
Surface Runoff	$mm{\cdot}y^{-1}$	232	237	1.79 %	156	−34 %	12 %
Interflow	$mm{\cdot}y^{-1}$	232	223	−3.77 %	278	24 %	12 %
ETa	$mm{\cdot}y^{-1}$	480	482	0.44 %	645	34 %	5 %
Baseflow	$mm{\cdot}y^{-1}$	194	190	−2.30 %	218	15 %	12 %
Groundwater Recharge	$mm{\cdot}y^{-1}$	236	231	−1.96 %	259	12 %	11 %
SWE	*mm*	282	283	0.34 %	149	−47 %	9 %
Soil Moisture	-	0.172	0.171	−0.30 %	0.172	0.21 %	1.48 %

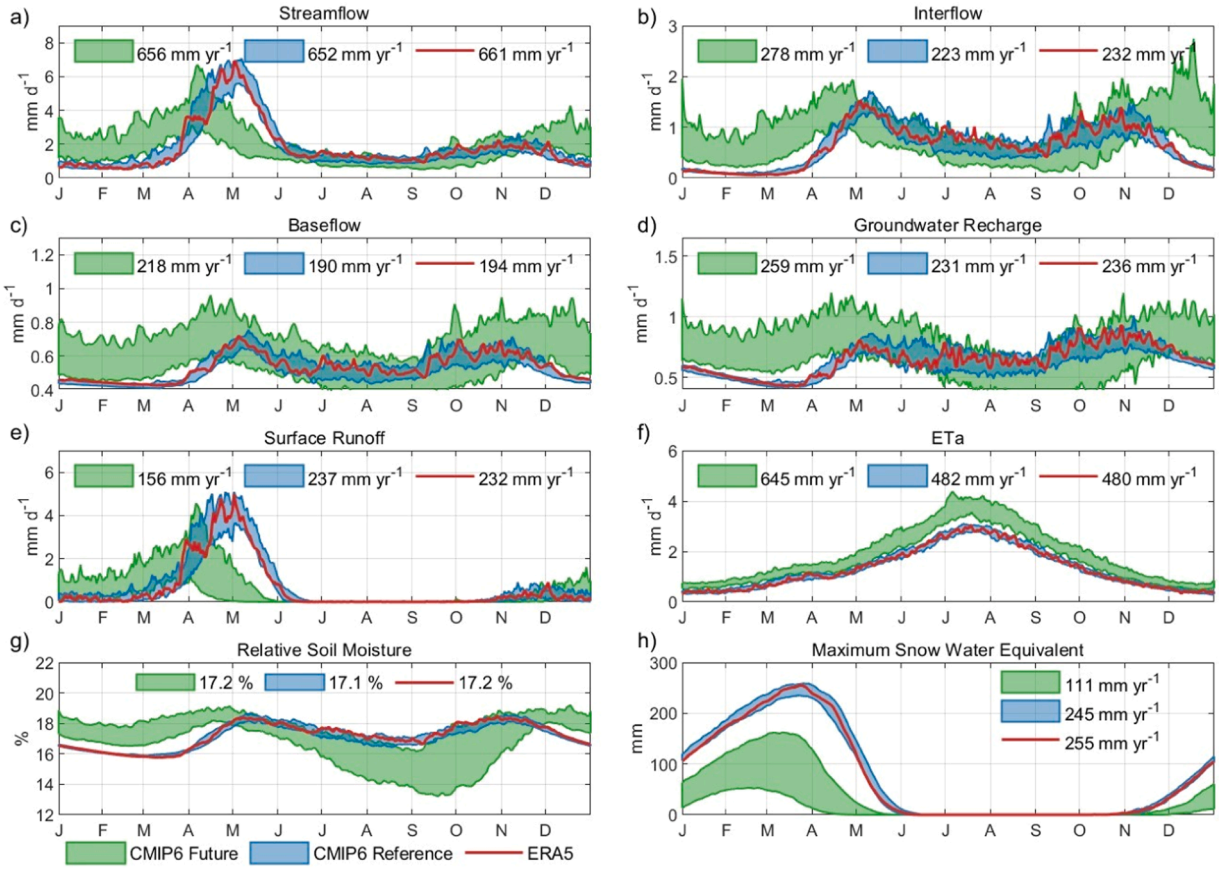

Fig. 5. Comparative analysis of annual dynamics of daily hydroclimatic variables across all catchments. Blue and green bands show the range of values simulated with CMIP6 data for the reference and future periods, respectively, while the red line represents simulations with ERA5 data for the reference period. Average simulated values for each period and dataset are shown next to legend symbols in each panel.

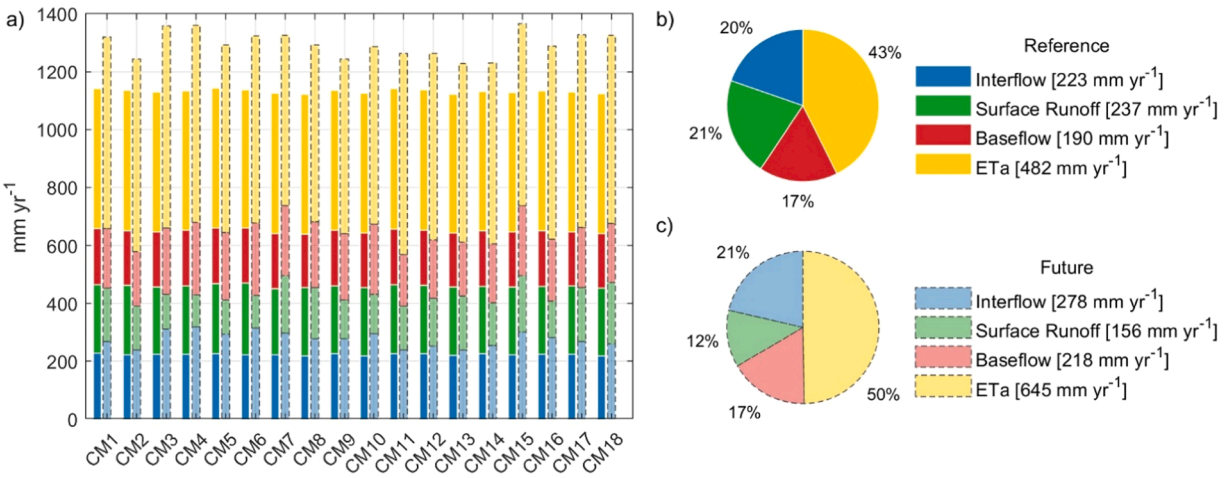

Fig. 6. Distribution of hydroclimatic variables for reference and future periods across eighteen climate models (CM1 to CM18). Panel (a) shows segmented bars for Interflow (blue), Surface Runoff (green), Baseflow (red), and Evapotranspiration (ETa, yellow), in millimeters per year (mm yr^{-1}). Panels (b) and (c) display pie charts illustrating proportional contributions of each process during the reference and future periods, respectively.

datasets, along with the minimal differences between climate models over the reference period, suggests the effectiveness of the bias-correction method. In contrast, the larger variance observed in the CMIP6 simulations for the future period suggests a higher uncertainty associated with the climate simulations in the future.

Comparisons between simulations driven by CMIP6 under reference and future periods reveals a noticeable shift in the timing of seasonal peak flow, moving from May to April, along with an increase in winter flows and a decrease in amplitude of the seasonal peak flow. Similar shifts also occur in interflow, baseflow, surface runoff, and groundwater recharge. Interflow, groundwater recharge, and soil moisture all show an increase during the colder months (November to May) and a slight decrease during the warmer months (June to October). Baseflow follows a similar pattern, with less pronounced decreases during the warmer months. Surface runoff largely increases between December and April. This change in runoff also coincides with a slight reduction in the amplitude of the peak related to snowmelt in the spring. Snow water equivalent consistently decreases throughout the year, which is also consistent with the decrease in snowfall precipitation (-33 %, Table 5). Actual evapotranspiration increases throughout the year, with a more substantial rise from June to September. This is due to higher temperatures during the summer months when water is no longer stored as ice or snow. In the boreal forests of the study area, transpiration is minimal in winter and at the end of autumn, and evaporation remains relatively low due to cold temperatures. However, in summer, higher temperatures increase potential evapotranspiration (ETP), leading to greater actual evapotranspiration (ETa) as the energy-limited system allows more water to be lost to the atmosphere. The wider range of values in future period simulations depicted variance related to the climate models.

Fig. 6 presents the contributions of hydroclimatic variables across all climate models for the reference and future periods. The similarity between climate models for all hydrological processes during the reference period is evident. However, there is increased variability between climate models in the future period, with surface runoff exhibiting the greatest variability. Figs. 6b and 6c reveal significant changes in the contributions of various processes between the two periods, such as an increase in ETa and interflow, and a decrease in surface runoff. Baseflow maintains a consistent proportion during both periods. The most notable changes occur in surface

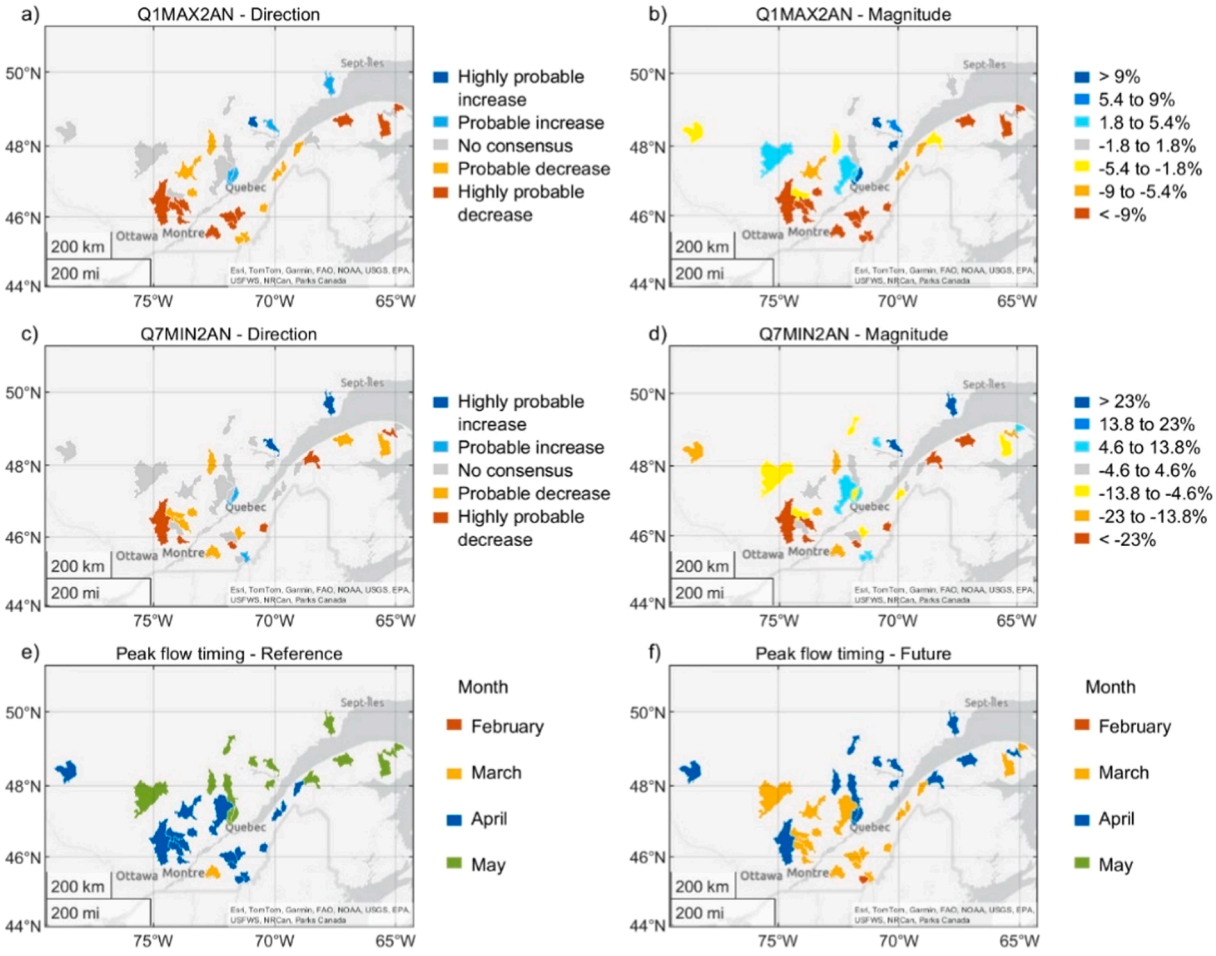

Fig. 7. Spatial distribution of changes in hydrological indicators and annual peak flow timing. Panels (a) and (b) show expected changes in direction and magnitude of annual maximum daily flow with a two-year return period. Panels (c) and (d) display expected changes in direction and magnitude of annual minimum 7-day mean flow. Panels (e) and (f) depict the seasonal distribution of annual peak flow timings during the reference and future periods, respectively.

runoff and ETa.

3.2.2. Streamflow

Fig. 7 illustrates the spatial pattern of the direction (increase or decrease) and the magnitude of change for the annual maximum daily flow with a two-year return period (panels 7a and 7b). Northeastern catchments predominantly exhibit an increase in maximum flow, while southwestern catchments indicate a decrease. This trend is reflected in the magnitude of changes, with the most southern and northern catchments displaying the highest magnitudes corresponding to their respective directions. Notably, catchments with the highest increases are small catchments with steep slopes.

The direction (increase or decrease) and the magnitude of change in the annual minimum 7-day mean flow with a two-year return period (panels 7c and 7d) indicate that almost all catchments show a decrease in flow, except for four catchments that exhibit a significant increase in flow magnitude, with three of them located on the North shore of the St-Lawrence River. Southeastern catchments generally present a higher magnitude of decrease, underscoring a clear spatial trend in the direction and extent of changes across the study area. Furthermore, many catchments show no consensus between climate models, suggesting variability between models and/or that the magnitude of change is close to zero leaving higher uncertainty on the potential impact of climate change in these catchments.

In addition to changes in the magnitude of minimum flows, a shift in the timing of annual minimum 7-day mean flow is also observed. In the future period, all catchments (except Godbout) experience their minimum flow during the summer. In contrast, for the reference period, the timing varies, with some catchments exhibiting their minimum flow in winter while others in summer, depending on the year. Notably, seven out of the 34 catchments show a clear shift from winter to summer minimum flows in the future period. This change has significant implications for water management, as winter minimum flows are projected to increase due to higher winter precipitation and reduced snow storage, while summer minimum flows are expected to decline due to increased

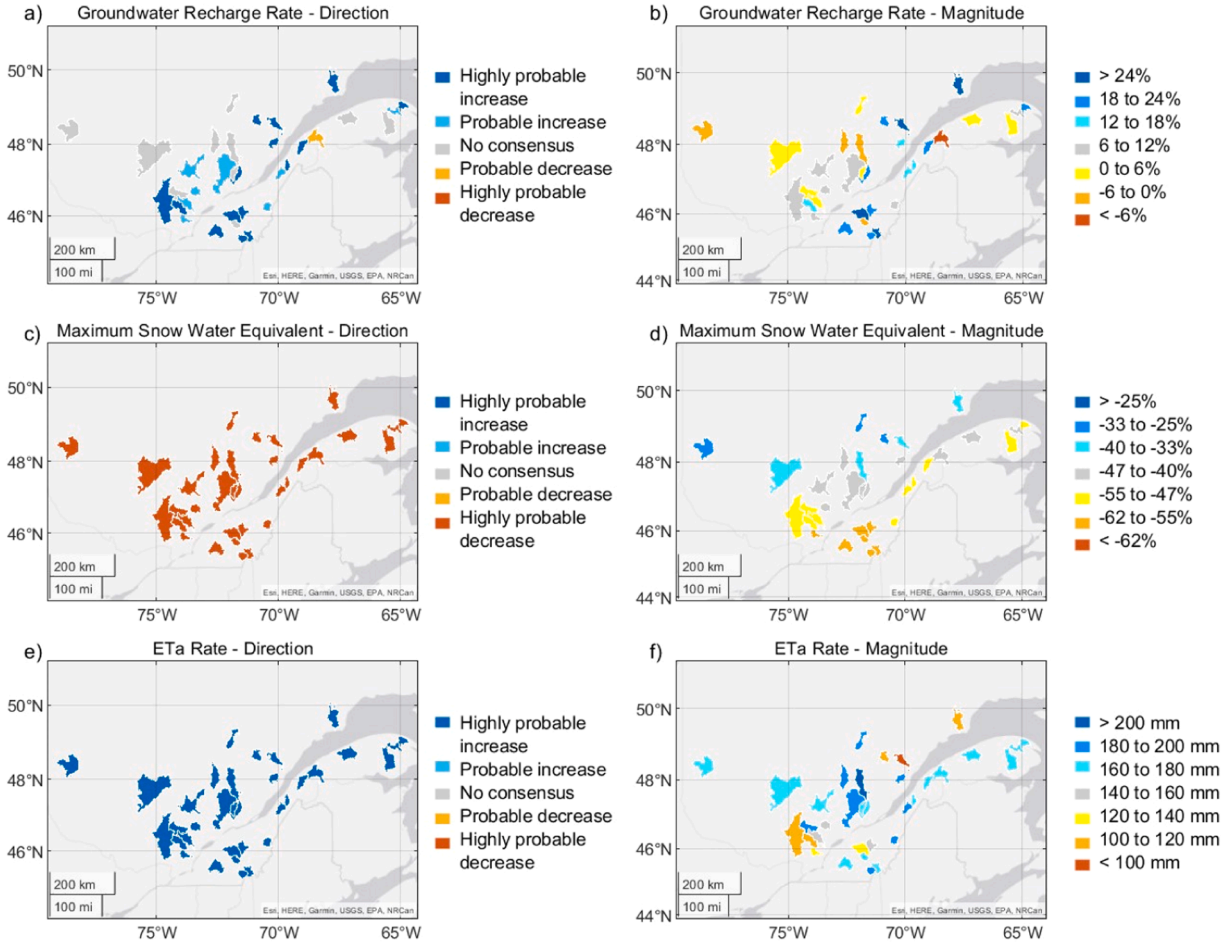

Fig. 8. Spatial distribution of changes in annual groundwater recharge rate, maximum snow water equivalent (SWE), and actual evapotranspiration rate (ETa). Panels (a) and (b) show expected changes in direction and magnitude of mean annual groundwater recharge rate. Panels (c) and (d) display expected changes in direction and magnitude of annual maximum SWE. Panels (e) and (f) depict expected changes in direction and magnitude of mean annual ETa rate.

evapotranspiration during the warm season.

The temporal shifts in annual peak flow (panels 7e and 7 f) highlight a noticeable trend toward earlier peak flows across many catchments, with a general shift of approximately one month. Catchments with peak flows traditionally occurring in May have shifted to April, while those with peak flows in April have moved to March. Notably, one southern catchment exhibits a peak flow in February. On average, the shift in peak flow timing across all catchments is 32 days, with a standard deviation of 8 days, indicating a significant and consistent temporal adjustment in peak flow timing.

3.2.3. Groundwater recharge, SWE and ETa

Fig. 8 indicate a general increase in groundwater recharge rates (panels 8a and 8b), with most catchments exhibiting an increase between 12 % and 24 %. There are no discernible spatial patterns in the distribution of these changes. One catchment shows an unexpected result with a highly probable decrease exceeding 6 %.

The results for the annual maximum SWE (panels 8c and 8d) indicate a clear decrease across all catchments, with magnitudes of change ranging between −25 % and −62 %. Catchments located in the southern part of the study area tend to exhibit higher magnitudes of decrease, while those further north show relatively lower magnitudes of change. The reduction in SWE is strongly correlated ($r = 0.94$) with a 44 % decrease in the average number of consecutive snow days, which drops from 167 days (standard deviation of 20 days) in the reference period to 94 days (standard deviation of 29 days) in the future period. Furthermore, the analysis of correlation coefficient reveals that higher temperature between December and March will decrease the number of consecutive snow days ($r = -0.89$), as expected.

The increase in temperature and precipitation leads to an increase in mean annual ETa across all catchments (panels 8e and 8 f), with magnitudes of change ranging between 95 and 203 millimeters. This result is expected because the catchments in the study area are energy-limited, meaning that higher temperatures provide more energy for evapotranspiration, leading to increased ETa. There is no distinct pattern in the spatial distribution of these changes, indicating that the increase in ETa is widespread and not confined to specific geographic areas within the study region.

3.3. Case study: Matane catchment

3.3.1. Hydroclimatic variables

The Matane catchment was selected for an in-depth case study analysis due to its representative characteristics of the study area. It serves as a valuable example for evaluating the impacts of climate change within the context of a snow-dominated catchment. The

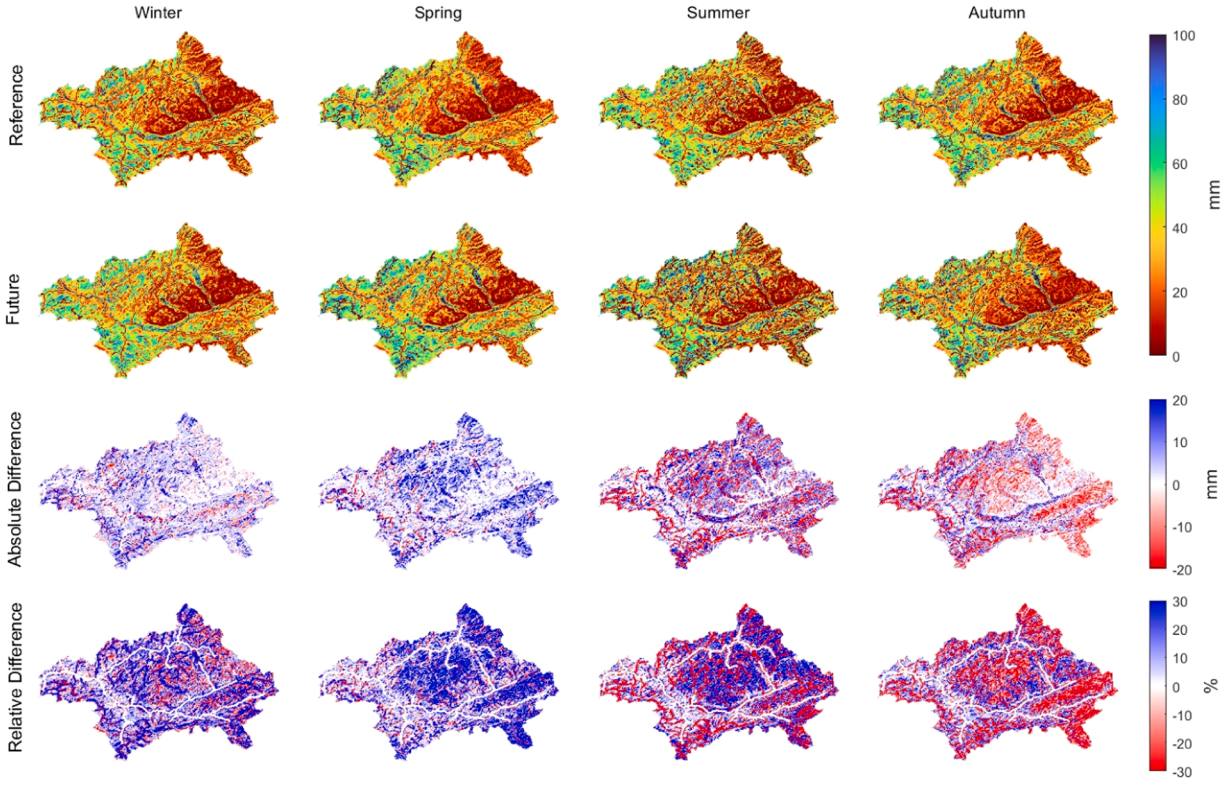

Fig. 9. Seasonal groundwater recharge rates in the Matane catchment, for reference and future periods (top two rows), and their differences (bottom two rows).

findings from the Matane catchment generally align with the broader regional patterns observed in the study, confirming its suitability as a representative case.

For instance, future projections indicate a significant increase in precipitation (42 %) and evapotranspiration (36 %) alongside a notable decrease in snowfall (-32 %) and snow water equivalent (-47 %). Similar trends were observed for streamflow, baseflow, interflow, and groundwater recharge, with increases during the colder months.

The Matane catchment also follows the regional trend of earlier seasonal peak flows, increased winter flows, and decreases in surface runoff during the spring peak period. These shifts in the timing and magnitude of hydrological processes reflect the broader impacts of climate change on the region's water cycle. The detailed results for the Matane catchment can be found in supplementary material, where Table S1 and Fig. S3 provide specific numerical comparisons and graphical representations of the annual dynamics of hydroclimatic variables.

3.3.2. Spatial variability of hydrological processes at the catchment scale

Fig. 9 shows the spatial distribution of groundwater recharge rates across the four seasons. It highlights the annual fluctuation in relative changes between the future and reference periods. There is notable spatial variation in groundwater recharge rates, consistent across both reference and future periods. The most significant spatial variation occurs during spring and summer, with some areas receiving up to 100 mm of recharge while others receive only 5 mm. Groundwater recharge rates closely follow the spatial variation in elevation throughout the catchment (Fig. S1 panel a), with higher elevations receiving less groundwater recharge while lower elevations receive more. Conversely, higher elevations received more interflow than lower elevations (Fig. S1).

The relative and absolute comparison allows for a better distinction of spatial and temporal variability and helps identify areas that are more prone to reductions. When examining the absolute and relative differences between the future and reference periods, winter and spring exhibit an increase in groundwater recharge rates across most of the catchment. Conversely, summer and autumn show a mix of increases and decreases, with both seasons predominantly experiencing decreases across the catchment. Spring receives the most significant absolute increase in groundwater recharge rates, with some areas experiencing increases close to 20 millimeters. In contrast, autumn sees the most substantial decrease in groundwater recharge rates, with certain parts of the catchment experiencing decreases of up to 20 millimeters.

Fig. 10 presents the spatial distribution of soil moisture across the four seasons. When comparing soil moisture with the soil type map of the catchment (Fig. S1 panel b), there is a clear relationship between soil type and soil moisture. Sandy loam soil, which is more permeable, has the lowest soil moisture levels, around 0.15. Loam soils exhibit soil moisture levels ranging from 0.25 to 0.3, while sandy clay soils have soil moisture levels between 0.3 and 0.35. Although the variability in soil moisture between seasons is small, it appears to be greater for the future period compared to the reference period.

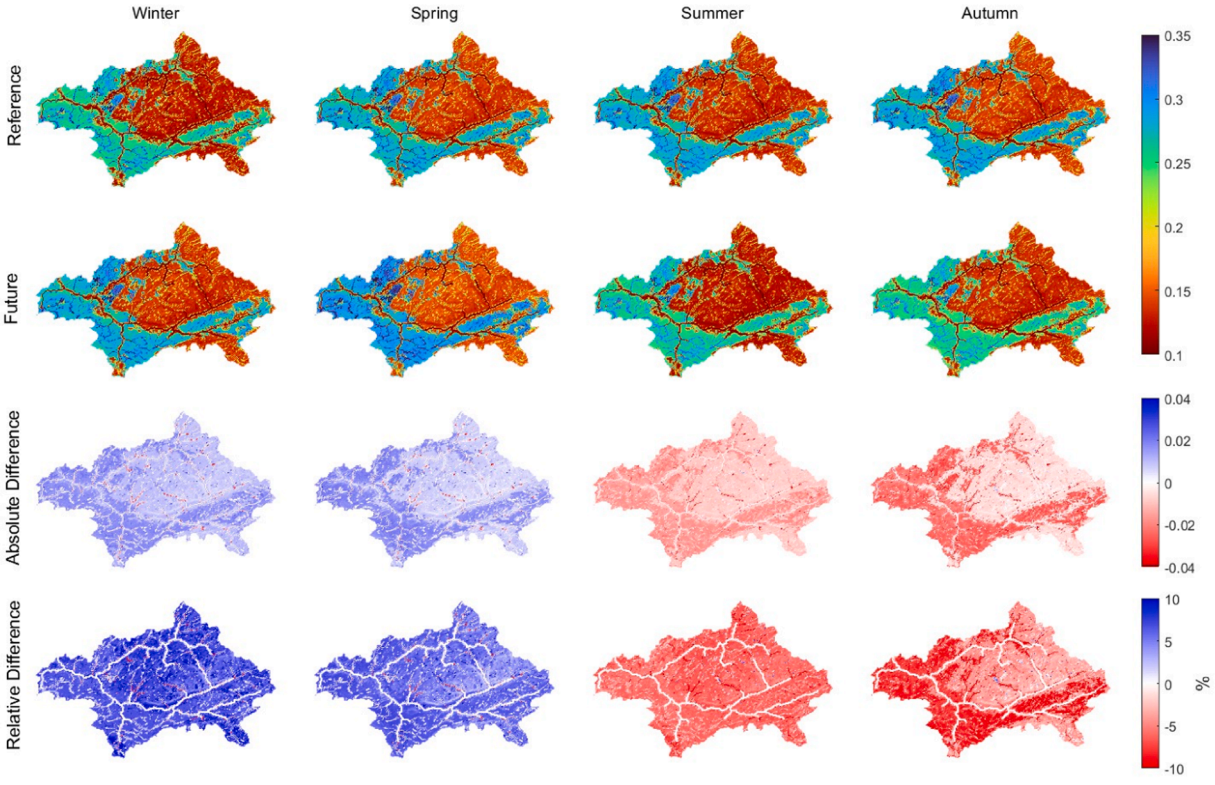

Fig. 10. Seasonal soil moisture in the Matane catchment, for reference and future periods (top two rows), and their differences (bottom two rows).

In terms of absolute and relative changes between the future and reference periods, winter and spring show an increase in soil moisture, while summer and autumn exhibit a decrease. These changes are relatively consistent across the entire catchment, with an absolute change of around 0.03 for all four seasons, depending on the direction of change.

4. Discussion

This study investigates the impacts of climate change on hydrological processes using a spatially distributed and physically based hydrological model, WaSiM, coupled with climate simulations from the SSP5–8.5, which represents a high greenhouse gas emissions scenario. The use of bias corrected CMIP6 climate model data for the future period indicates an increase in total precipitation, particularly pronounced from November to April, along with a significant temperature rise of five to eight degrees Celsius, depending on the climate model. In the following sections, results will be analyzed in terms of the various hydroclimatic variables.

4.1. Regional hydrological changes

4.1.1. Snow water equivalent

Projected changes in total precipitation indicate a 15 % increase relative to the reference period. However, rising temperatures will result in a 33 % decrease in snowfall, with more precipitation falling as rain instead of snow. This is in line with the 20 % reduction found by Nolin et al., (2023) for the Upper Harricana River, but less than the 50 % reduction in snowfall highlighted in Valencia Giraldo et al. (2023) for the five degrees Celsius warming scenario. This shift leads to a shorter snow accumulation period, with the average number of consecutive snow days projected to decrease significantly, averaging 94 days (standard deviation of 29 days) in the future compared to 167 days (standard deviation of 20 days) in the reference period. This 44 % reduction in mean number of snow days is consistent with the 45 % reduction for the + 6°C scenarios reported by (Valencia Giraldo et al., 2023).

Additionally, the results showed a corresponding decrease in SWE between 25 % and 62 %, representing a 4–11 % reduction in SWE per °C, depending on the latitude of the catchment. This is less than the 25 %-35 % reduction per °C for the 0–2 °C warming zone found by (Aygün et al., 2020b) and the 69 % decrease found by Cochand et al. (2019), but aligns with the 2.5–7.5 % reduction per decade for Southern Quebec highlighted by Mudryk et al. (2018), and the 43 % reduction found by Novotná et al. (2013).

Catchments in the southern part of the study area show larger decreases in SWE magnitudes (Fig. 8 panel c), whereas those further north exhibit relatively smaller changes—a trend also present in Mudryk et al. (2018). This reduction in SWE is strongly correlated with the absolute change in consecutive snow days ($r = 0.94$). Furthermore, the analysis reveals a strong negative correlation ($r = -0.89$) between the absolute change in consecutive snow days and the mean temperature during the months of December to March in the future period. This suggests that the reduction in consecutive snow days is due to higher temperatures in the southern catchments, bringing them closer to the melting point. Consequently, increases in winter temperatures are a significant factor driving the reduction in snow days and the decrease in SWE. This occurred despite a significant increase in winter precipitation, indicating that more precipitation is falling as rain rather than snow.

4.1.2. Actual evapotranspiration

For the reference period, the model produced a mean actual evapotranspiration (ETa) of approximately 480 mm per year, with higher ETa values observed in the southern catchments of the study region. Although direct observational datasets for ETa are limited, we compared simulated potential evapotranspiration (ETP) values with publicly available estimates from Natural Resources Canada (Natural Resources Canada, 2023). The simulated ETP values exhibited a similar spatial pattern, with higher values in the south and lower values in the north, consistent with expectations based on temperature gradients. The study reveals a change in ETa, increasing from 95 to 203 millimeters, with no distinct pattern in the spatial variability of these changes across the catchments. This aligns with results in Valencia Giraldo et al. (2023) under the 6 degrees Celsius warming scenario, and the 96 millimeters increase found by Novotná et al. (2013). This widespread increase suggests that the factors driving this increase are not localized but affect the entire study area uniformly. One significant factor contributing to this increase is the rise in temperature, which increases the modelled rate of potential evapotranspiration. Furthermore, the contribution of ETa to the water cycle is projected to grow substantially. Currently, ETa accounts for 43 % of the total water cycle. However, according to our simulation, this rate is expected to rise to 50 % in the future. This trend is also highlighted in Valencia Giraldo et al. (2023) under the 6 degrees Celsius warming scenario. This shift raises questions on how such increases in evapotranspiration will impact hydrological processes under future conditions. Higher temperatures increase the potential for water loss through evapotranspiration, leading to a greater proportion of the total precipitation being returned to the atmosphere rather than contributing to runoff and interflow, ultimately impacting streamflow. Additionally, the increase in total precipitation combined to shorter winter period could make more water available for evaporation, further contributing to the rise in ETa.

While this study focuses on ETa, it is important to differentiate it from potential evapotranspiration (ETP), as discussed in other studies (Dallaire et al., 2021). ETP represents the maximum possible evapotranspiration under ideal conditions, whereas ETa provides a better approximation of the actual water loss from land surfaces and vegetation.

The focus on ETa in this study is more useful for informing decision-makers about water availability. ETa reflects the actual conditions in the catchment, considering the availability of water and the specific characteristics of the landscape and vegetation. This makes ETa a more practical measure for assessing the impacts of climate change on water resources and for developing effective water management strategies.

4.1.3. Streamflow

Higher temperatures and increased winter precipitation in the future lead to more precipitation falling as rain rather than snow, enhancing streamflow from December to April. This change could be associated with earlier and lower peak flow during the year, shifting by an average of 32 days across all catchments. This shift is less than the three-month shift found by Aygün et al. (2020b) but aligns with the worst emission scenario peak discharge shift reported by Cochand et al. (2019) and the results presented by Gombault et al. (2015) and Minville et al. (2008). The shift in timing of peak flows from spring to earlier in the year is due to the reduced snowpack and earlier snowmelt, a consequence of rising temperatures.

The maximum daily flow with a 2-year return period shows changes between −26 % and 15 %, with most catchments showing changes between −9 % and 9 %. These results align with the median decrease of 10–15 % in spring high flows with a 5-year return period found by Riboust and Brissette (2015). Northern catchments predominantly exhibit an increase in maximum flow, while southern catchments indicate a decrease, consistent with the findings in the Hydroclimatic Atlas of Southern Québec (2022). The relative change in maximum flow is correlated with the relative change in SWE ($r = 0.76$). Southern catchments show a stronger decrease in high flows due to their significant decrease in SWE. Conversely, northern catchments present a smaller magnitude of decrease and even an increase in high flows due to a modest reduction in SWE and an increase in total precipitation. Notably, catchments with the highest increases in streamflow are small northern catchments with steep slopes, where the reduction of SWE was modest and heavy rain could rapidly reach the outlet.

The minimum 7-day flow with a 2-year return period shows changes between −44–42 %, with most catchments showing changes between −23 % and 23 %. These results align with the findings in Valencia Giraldo et al. (2023) and the Hydroclimatic Atlas of Southern Québec (2022). Most southern catchments present a decrease in low flows, while two northern catchments exhibit a strong increase. For the latter, minimum flows typically occur during the winter low-flow period. With the reduction of SWE and the increase in rainfall, winter low flows are expected to be less intense, resulting in increased minimum flows during winter. This contrasts with southern catchments, where low flows occur during the summer months. With the increase in evapotranspiration, it is expected that summer low flows will decrease. Additionally, the results indicate a shift in the timing of minimum flows, with several catchments having their annual minimum flow transitioning from winter to summer in the future period. This shift may have significant implications for water availability particularly in regions where summer low flows are already a limiting factor.

Significant changes are observed across streamflow components for the future period. Annual surface runoff shows a 34 % decrease, contrasting with the 11–21 % increase found by Gombault et al. (2015). This reduction in surface runoff is linked to decreased snowfall and snowmelt, consistent with findings in Talbot et al. (2024a). The timing of peak surface runoff shifts earlier in the year, corresponding with the change in peak flow timing, and an increase in surface runoff is observed from December to April due to snow melt during these months. Surface runoff's contribution to hydrological processes decreases from 21 % during the reference period to 12 % in the future, indicating a reduced role of surface runoff in the overall water cycle.

4.1.4. Soil moisture

Projected changes in soil moisture reflect a nuanced interplay between increased precipitation, temperature rise, and changes in evapotranspiration rates. For the future, our results show a small increase in soil moisture from December to April and a small decrease from May to November relative to reference conditions.

In the winter months, increases in soil moisture are primarily driven by higher temperatures and increased precipitation. Higher temperatures reduce snow cover and soil freezing depth, allowing water to infiltrate the soil more effectively (Lundberg et al., 2016). This is corroborated by a strong correlation ($r = 0.79$) between soil moisture absolute change and winter temperature increase, as well as by the correlation ($r = 0.67$) with the absolute increase in rainfall during winter. The reduction in soil freezing along with higher winter precipitation enable more water to be retained in the soil, increasing soil moisture levels during these months.

From May to November, soil moisture decreases. Since the catchments are energy-limited and not water-limited, higher temperatures increase the modelled rate of potential evapotranspiration, leading to greater evapotranspiration and a reduction in soil moisture. The relative decrease in soil moisture is closely related to the relative increase in ETa, with correlation coefficients of 0.81 in summer and 0.79 in autumn. As temperatures rise, more water is lost through evapotranspiration, reducing the amount of water available to infiltrate the soil. Sulis et al. (2011) and Houle et al. (2012) found similar patterns in soil moisture variability, with increases during winter and spring and decreases in summer and autumn, influenced by topographic and pedologic characteristics.

In the distributed results for the Matane Catchment, soil moisture values range from 0.1 to 0.35, depending on the area. Soil moisture levels are closely related to the saturated hydraulic conductivity of the major soil types of each catchment, with a correlation coefficient r of 0.70. Furthermore, absolute changes in soil moisture and groundwater recharge are positively correlated, with an r value of 0.71. This relationship underscores the interconnectedness of soil moisture and groundwater recharge processes, particularly in response to changes in precipitation and evapotranspiration.

4.1.5. Groundwater recharge rate

The annual groundwater recharge rate is projected to increase across most catchments, ranging from 6 % to over 24 %. Temporally, groundwater recharge rates rise from December to May and decrease from July to November compared to the reference period. This temporal pattern is influenced by seasonal variations in precipitation, temperature, and evapotranspiration.

In winter and spring, the increase in groundwater recharge is driven by higher precipitation and lower evapotranspiration compared to the summer months. The higher winter precipitation and reduced soil freezing allow more water to infiltrate and recharge the groundwater. These findings align with Sulis et al. (2011), who observed similar seasonal variations in the Anglais River basin, where winter recharge increased by 49 % due to more rain and snowmelt.

Conversely, in summer and autumn, groundwater recharge rates vary, showing both increases and decreases across the catchments. Decreases in groundwater recharge during these seasons are closely correlated with increased evapotranspiration rates. As temperatures rise, more water is lost to evapotranspiration, reducing the amount available for groundwater recharge. This is supported by a strong correlation ($r = -0.71$) between the absolute change in summer ETa and the absolute change in summer recharge. Higher evapotranspiration rates during summer outweigh the increase in precipitation, leading to a net decrease in groundwater recharge. Similar trends were noted by Cochand (2014) in the Saint-Charles River watershed, where summer recharge decreased due to increased evapotranspiration.

For the Matane Catchment, the spatial distribution of groundwater recharge rates varies significantly across the four seasons. Spring exhibits the largest increase, with some areas experiencing rises of up to 20 millimeters. In contrast, autumn shows the greatest decrease, with reductions of up to 20 millimeters. These variations are influenced by the catchment's topography, highlighting the importance of using high-resolution spatial data in hydrological modeling. Dubois et al. (2022) emphasized the need for detailed spatial analysis to accurately capture such variations in groundwater recharge. Other studies in cold and humid climates or regions with snow-dependent hydrology have reported similar patterns of increased winter recharge and decreased summer recharge (Grinevskiy et al., 2021; Wright and Novakowski, 2020). These studies consistently highlight the significant impact of warmer winters and increased winter liquid precipitation on enhancing groundwater recharge during colder months, while higher summer temperatures and evapotranspiration rates reduce recharge during warmer months.

The spatial variability in groundwater recharge rates is closely linked to elevation. Higher elevations tend to receive less groundwater recharge, while lower elevations receive more. This is reflected in a mean correlation coefficient r of -0.74 (std $= 0.19$) between the future period recharge of each sub-catchments and their corresponding mean elevation.

Interestingly, these findings contrast with those of Lindquist et al. (2019), who observed a positive relationship between groundwater recharge and elevation, as well as Sulis et al. (2011), who noted that the strongest responses in relative recharge changes were observed at higher elevations. The discrepancy may be attributable to our specific methodological approach, particularly the soil thickness separation we incorporated. In our study, higher elevations had thinner soil layers, while lower elevations had thicker soil layers, potentially influencing recharge rates.

These results emphasize the importance of considering soil thickness in hydrological studies, as it can significantly impact groundwater recharge dynamics. The differences observed in our study suggest that other research might have overlooked this critical factor, leading to differing results. These findings highlight the need for a comprehensive representation of physical soil attributes in hydrological models to better understand and predict groundwater recharge under future climate scenarios.

It is important to critically examine these results and consider that the observed differences might stem from the structural characteristics of the WaSiM model. The model's configuration, including the way soil thickness was assigned based on elevation, might introduce biases that differ from other studies. Therefore, while our findings contribute to the understanding of groundwater recharge dynamics under future climate scenarios, they also highlight the need for cautious interpretation and further investigation into the model's assumptions and configurations.

4.2. Benefits and limitations

This study aims to evaluate the hydrological impacts of climate change using a physically based, spatially distributed hydrological model (WaSiM) and the latest CMIP6 climate projections. The key objectives include understanding future hydroclimatic conditions, improving water resources management, and enhancing adaptive strategies.

The primary benefit of using a physically based, spatially distributed model like WaSiM is its ability to capture local heterogeneity and finer-scale processes. This is particularly important for boreal regions like Quebec, which experience diverse and complex hydrological dynamics. The use of multiple General Circulation Models (GCMs) within the CMIP6 framework provides a more comprehensive representation of potential future climatic conditions, thereby reducing the uncertainty associated with a single model approach.

Additionally, the use of an advanced bias-correction method, MBCn, enhances the robustness of climate projections by maintaining inter-variable correlations and spatiotemporal patterns. This approach ensures that the modeled hydrological responses are more reflective of the actual climatic conditions, thus providing valuable insights for water resources management. By focusing on a high-resolution spatial and temporal analysis, the study provides detailed insights into the seasonal and spatial variability of hydrological processes. This level of detail is crucial for understanding how different parts of the catchments will respond to climate change, aiding in more targeted and effective management practices.

Despite its strengths, this study has limitations that need to be addressed in future research. One limitation is the reliance on a single Shared Socioeconomic Pathway (SSP) scenario. While this study focused on the worst-case SSP5–8.5 scenario to highlight potential extreme impacts, incorporating multiple SSP scenarios would provide a more comprehensive view of potential future climatic conditions and their impacts on hydrological processes. Another limitation is the use of only one hydrological model. Although WaSiM is well-suited for capturing spatiotemporal dynamics, employing multiple hydrological models would provide a more nuanced understanding of hydrological responses and reduce model-related uncertainty. However, this approach would significantly increase computational time and resources.

The calibration of only one set of parameters per catchment introduces additional uncertainty. Despite the model demonstrating strong validation performance along with the use of an integrated calibration approach that enhances the representation of catchment hydrological processes (Talbot et al., 2024a), using multiple parameter sets could offer a more comprehensive assessment of the sensitivity and variability of the hydroclimatic variables. However, this would also cause an increase in computational time and

complexity. Furthermore, the spatial and temporal resolution of the model, although effective, may overlook some finer-scale processes. Increasing these resolutions could provide more detailed insights, particularly in heterogeneous landscapes and during extreme short-time meteorological events. Nevertheless, this would also result in increased computational time.

Several methodological choices introduce potential sources of uncertainty in this study. One limitation is the calibration period, which was restricted to 10 years due to computational constraints. While this period was found to be a good balance between robustness and feasibility, a longer calibration period could further improve model reliability. Additionally, the WaSiM model configuration may overestimate surface runoff in some catchments, as observed in the Eaton catchment, characterized by a high proportion of cropland, where snowmelt-generated runoff was overly reactive. The use of ERA5 data for historical meteorological inputs instead of alternative reanalysis products is another potential source of bias, as different datasets may influence model forcing and subsequent simulations. Furthermore, uncertainties stem from the CMIP6 climate models and the bias correction methods applied, as different models and correction techniques can yield varying hydrological projections. Lastly, the number of evaluations in the calibration process could also impact model performance, as additional iterations might lead to further parameter refinement. These factors highlight the inherent uncertainties in climate change impact assessments and emphasize the need for careful interpretation of results.

This research provides a rare and detailed assessment of climate change impacts on hydrology across 34 catchments in Southern Quebec, offering valuable insights into how multiple components of the water cycle respond to changing climatic conditions. By analyzing a wide range of hydrological variables such as rainfall, snowfall, snow water equivalent, evapotranspiration, soil moisture, surface runoff, and groundwater recharge, this study captures not only the magnitude of individual changes but also the evolving relationships among these processes. These findings are particularly relevant in cold and snowy regions where hydrological dynamics are strongly influenced by seasonal shifts and snow-dominated regimes. The observed patterns and interactions across physiographically diverse catchments enhance the generalizability of the results and support more informed adaptation strategies. This integrated and multi-variable approach reinforces the importance of considering hydrological processes as an interconnected system rather than in isolation when assessing the impacts of climate change on water resources.

Having spatially distributed results is crucial for identifying regions at risk, understanding hydrological dynamics, and developing targeted water management strategies. The spatially explicit modeling approach allows for the identification of specific areas that may be more vulnerable to changes in precipitation, snow cover and depth, soil moisture, and groundwater recharge. This detailed information can guide the implementation of adaptive measures, such as improving infrastructure resilience, protecting critical habitats, and ensuring sustainable water supply.

Overall, the hydrological shifts projected in this study will have significant implications for multiple sectors, necessitating adaptation strategies to mitigate potential risks. The projected reduction in snowfall will pose significant challenges for ski resorts and the winter tourism industry, as shorter snow seasons and reduced snow cover may impact their operations and economic viability. Additionally, increasing evapotranspiration, lower summer low flows, and reduced soil moisture are expected to negatively affect agricultural productivity, ecosystems, and vegetation sensitive to summer droughts. These changes will likely necessitate improved irrigation systems and adaptive land management strategies to mitigate the risks associated with drier conditions. At the same time, higher winter flows may provide some advantages for hydroelectric reservoir management, as water that was historically stored as snow will now become available earlier in the season. This shift could facilitate reservoir recharge but may also require adjustments in seasonal storage strategies to ensure long-term water availability. However, more intense winter and spring streamflows could also lead to an increased risk of flooding, emphasizing the need for enhanced flood mitigation measures and infrastructure adaptations to manage potential hydrological extremes. Hydrological changes will impact forest management, as shifting soil moisture and temperature conditions affect tree growth and regeneration.

Given these sectoral impacts, studies that assess multiple hydrological processes under climate change scenarios are crucial. Effective adaptation requires robust quantification of future climate impacts, and hydrological models play a key role in simulating essential variables such as precipitation, river discharge, groundwater recharge, and evapotranspiration. These projections are indispensable for anticipating climate change impacts and guiding sustainable water resource and forestry management. For instance, accurate soil moisture simulations would help optimizing irrigation and maintaining crop yields. Equally, spatially continuous information on soil moisture could help identifying sites that are more vulnerable to drought which in turn will help refining forest management strategies under future climate conditions. On the other hand, groundwater recharge modeling is critical for securing potable water supplies and managing aquifers sustainably, while surface runoff simulations are vital for urban infrastructure planning and flood prevention.

In addition to these considerations, future research could benefit from a retrospective analysis of historical water balance trends to detect and attribute past hydrological changes to climate drivers. Linking such observational insights with model projections would strengthen the understanding of climate change impacts on the water cycle and provide a valuable reference point for validating future scenarios. Furthermore, incorporating snow-related observations such as snow cover and snow depth into the calibration framework could improve the representation of key seasonal processes, particularly in snow-dominated catchments. While such integration remains challenging due to limited spatial coverage and the need for validation of satellite-derived products, recent advances in deep learning approaches (Demil et al., 2025) offer promising alternatives to help reduce these limitations in the future.

5. Conclusion

This study comprehensively assessed the impacts of climate change on hydroclimatic variables in Quebec using a physically based, spatially distributed hydrological model (WaSiM) and CMIP6 climate projections. The findings reveal significant changes in snow

water equivalent, evapotranspiration, groundwater recharge, soil moisture, and streamflow dynamics under future climate scenarios.

Key results indicate a considerable increase in total precipitation and temperature, leading to a shift from snowfall to rainfall, reduced snowpack, and earlier snowmelt. This change is expected to cause a seasonal shift in the timing of peak flows and an increase in winter minimum flows. Additionally, the study highlights a significant increase in groundwater recharge rates during the winter and spring months, attributed to higher precipitation and reduced soil freezing.

This research underscores the importance of employing advanced modeling techniques and the latest climate projections to enhance our understanding of climate change impacts on hydrology. The methodologies and findings are not only pertinent to Quebec but also applicable to other regions with similar climatic and hydrological conditions, such as parts of Europe, North America, and Asia. By providing a more accurate and comprehensive assessment of future hydrological changes, this study supports more informed decision-making and adaptive management practices to mitigate the impacts of climate change on water resources and ecosystems globally.

Funding

This work was funded jointly by the Ministère des Ressources naturelles et des Forêts (Quebec, Canada, project number 112332187 conducted at the Direction de la recherche forestière and led by Jean-Daniel Sylvain) and the Forest Research Service contract number 3322–2022–2187–01 obtained by Richard Arsenault from the Ministère des Ressources naturelles et des Forêts (Quebec, Canada).

CRediT authorship contribution statement

Sylvain Jean-Daniel: Writing – review & editing, Supervision, Project administration, Methodology, Funding acquisition, Conceptualization. **Talbot Frédéric:** Writing – review & editing, Writing – original draft, Validation, Software, Methodology, Investigation, Formal analysis, Data curation, Conceptualization. **Poulin Annie:** Writing – review & editing. **Drolet Guillaume:** Writing – review & editing. **Arsenault Richard:** Writing – review & editing, Project administration, Methodology, Funding acquisition, Conceptualization. **Martel Jean-Luc:** Writing – review & editing, Software.

Declaration of Generative AI and AI-assisted technologies in the writing process

During the preparation of this work the author(s) used ChatGPT-4 for assistance in correcting spelling mistakes and improving the flow of text during the manuscript preparation process. After using this tool/service, the author(s) reviewed and edited the content as needed and take(s) full responsibility for the content of the published article.

Declaration of Competing Interest

The authors declare that they have no known competing financial interests or personal relationships that could have appeared to influence the work reported in this paper.

Acknowledgements

The base map in Fig. 1 was created using ArcGIS® software by Esri. ArcGIS® and ArcMap™ are the intellectual property of Esri and are used herein under license. Copyright © Esri. All rights reserved. For more information about Esri® software, please visit www.esri.com.

Appendix A. Supporting information

Supplementary data associated with this article can be found in the online version at doi:10.1016/j.ejrh.2025.102453.

Data availability

The calibrated WaSiM model and all simulations for all catchments discussed in this study are publicly accessible at https://osf.io/d9wze/ (Talbot et al., 2024b).

References

Arsenault, R., Brissette, F., Chen, J., Guo, Q., Dallaire, G., 2020. NAC2H: The North American Climate Change and Hydroclimatology Data Set. e2020WR027097 Water Resour. Res. 56. https://doi.org/10.1029/2020WR027097.

Arsenault, R., Poulin, A., Côté, P., Brissette, F., 2014. Comparison of Stochastic Optimization Algorithms in Hydrological Model Calibration. J. Hydrol. Eng. 19, 1374–1384. https://doi.org/10.1061/(ASCE)HE.1943-5584.0000938.

Aygün, O., Kinnard, C., Campeau, S., 2020a. Impacts of climate change on the hydrology of northern midlatitude cold regions. Prog. Phys. Geogr.: Earth Environ. 44, 338–375. https://doi.org/10.1177/0309133319878123.

Aygün, O., Kinnard, C., Campeau, S., Krogh, S.A., 2020b. Shifting Hydrological Processes in a Canadian Agroforested Catchment due to a Warmer and Wetter Climate. Water 12, 739. https://doi.org/10.3390/w12030739.

Beck, H.E., Zimmermann, N.E., McVicar, T.R., Vergopolan, N., Berg, A., Wood, E.F., 2018. Present and future Köppen-Geiger climate classification maps at 1-km resolution. Sci. Data 5, 180214. https://doi.org/10.1038/sdata.2018.214.

Beven, K., 2001. How far can we go in distributed hydrological modelling. Hydrol. Earth Syst. Sci. 5, 1–12. https://doi.org/10.5194/hess-5-1-2001.

Blöschl, G., Sivapalan, M., 1995. Scale issues in hydrological modelling: A review. Hydrol. Process. 9, 251–290. https://doi.org/10.1002/hyp.3360090305.

Bormann, H., Elfert, S., 2010. Application of WaSiM-ETH model to Northern German lowland catchments: model performance in relation to catchment characteristics and sensitivity to land use change, in: Advances in Geosciences. Presented at the Hydrologic Modelling for the Assessment of Ecosystem Services and Landscape Functions - 3th Workshop "Large-scale Hydrological Modelling – Hydrological Modelling for the Assessment of Ecosystem Services and Landscape Functions", Dresden, Germany, 25–27 November 2009, Copernicus GmbH, pp. 1–10. ⟨https://doi.org/10.5194/adgeo-27-1-2010⟩.

Boucher, O., Servonnat, J., Albright, A.L., Aumont, O., Balkanski, Y., Bastrikov, V., Bekki, S., Bonnet, R., Bony, S., Bopp, L., Braconnot, P., Brockmann, P., Cadule, P., Caubel, A., Cheruy, F., Codron, F., Cozic, A., Cugnet, D., D'Andrea, F., Davini, P., de Lavergne, C., Denvil, S., Deshayes, J., Devilliers, M., Ducharne, A., Dufresne, J.-L., Dupont, E., Éthé, C., Fairhead, L., Falletti, L., Flavoni, S., Foujols, M.-A., Gardoll, S., Gastineau, G., Ghattas, J., Grandpeix, J.-Y., Guenet, B., Guez, E., Lionel, Guilyardi, E., Guimberteau, M., Hauglustaine, D., Hourdin, F., Idelkadi, A., Joussaume, S., Kageyama, M., Khodri, M., Krinner, G., Lebas, N., Levavasseur, G., Lévy, C., Li, L., Lott, F., Lurton, T., Luyssaert, S., Madec, G., Madeleine, J.-B., Maignan, F., Marchand, M., Marti, O., Mellul, L., Meurdesoif, Y., Mignot, J., Musat, I., Ottlé, C., Peylin, P., Planton, Y., Polcher, J., Rio, C., Rochetin, N., Rousset, C., Sepulchre, P., Sima, A., Swingedouw, D., Thiéblemont, R., Traore, A.K., Vancoppenolle, M., Vial, J., Vialard, J., Viovy, N., Vuichard, N., 2020. Presentation and Evaluation of the IPSL-CM6A-LR Climate Model. e2019MS002010 J. Adv. Model. Earth Syst. 12. https://doi.org/10.1029/2019MS002010.

Buffin-Bélanger, T., Chaillou, G., Cloutier, C.-A., Touchette, M., Hétu, B., McCormack, R., 2015. Programme d'acquisition de connaissance sur les eaux souterraines du nord-est du Bas-Saint-Laurent (PACES-NEBSL): Rapport final. Université du Québec à Rimouski, Département de biologie, chimie et géographie, Rimouski, Québec.

Calvin, K., Dasgupta, D., Krinner, G., Mukherji, A., Thorne, P.W., Trisos, C., Romero, J., Aldunce, P., Barrett, K., Blanco, G., Cheung, W.W.L., Connors, S., Denton, F., Diongue-Niang, A., Dodman, D., Garschagen, M., Geden, O., Hayward, B., Jones, C., Jotzo, F., Krug, T., Lasco, R., Lee, Y.-Y., Masson-Delmotte, V., Meinshausen, M., Mintenbeck, K., Mokssit, A., Otto, F.E.L., Pathak, M., Pirani, A., Poloczanska, E., Pörtner, H.-O., Revi, A., Roberts, D.C., Roy, J., Ruane, A.C., Skea, J., Shukla, P.R., Slade, R., Slangen, A., Sokona, Y., Sörensson, A.A., Tignor, M., Van Vuuren, D., Wei, Y.-M., Winkler, H., Zhai, P., Zommers, Z., Hourcade, J.-C., Johnson, F. X., Pachauri, S., Simpson, N.P., Singh, C., Thomas, A., Totin, E., Arias, P., Bustamante, M., Elgizouli, I., Flato, G., Howden, M., Méndez-Vallejo, C., Pereira, J.J., Pichs-Madruga, R., Rose, S.K., Saheb, Y., Sánchez Rodríguez, R., Ürge-Vorsatz, D., Xiao, C., Yassaa, N., Alegría, A., Armour, K., Bednar-Friedl, B., Blok, K., Cissé, G., Dentener, F., Eriksen, S., Fischer, E., Garner, G., Guivarch, C., Haasnoot, M., Hansen, G., Hauser, M., Hawkins, E., Hermans, T., Kopp, R., Leprince-Ringuet, N., Lewis, J., Ley, D., Ludden, C., Niamir, L., Nicholls, Z., Some, S., Szopa, S., Trewin, B., Van Der Wijst, K.-I., Winter, G., Witting, M., Birt, A., Ha, M., Romero, J., Kim, J., Haites, E.F., Jung, Y., Stavins, R., Birt, A., Ha, M., Orendain, D.J.A., Ignon, L., Park, S., Park, Y., Reisinger, A., Cammaramo, D., Fischlin, A., Fuglestvedt, J. S., Hansen, G., Ludden, C., Masson-Delmotte, V., Matthews, J.B.R., Mintenbeck, K., Pirani, A., Poloczanska, E., Leprince-Ringuet, N., Péan, C., 2023. IPCC, 2023: Climate Change 2023: Synthesis Report. Contribution of Working Groups I, II and III to the Sixth Assessment Report of the Intergovernmental Panel on Climate Change [Core Writing Team, H. Lee and J. Romero (eds.)]. IPCC, Geneva, Switzerland. Intergovernmental Panel on Climate Change (IPCC). ⟨https://doi.org/10.59327/IPCC/AR6-9789291691647⟩.

Cannon, A.J., 2018. Multivariate quantile mapping bias correction: an N-dimensional probability density function transform for climate model simulations of multiple variables. Clim. Dyn. 50, 31–49. https://doi.org/10.1007/s00382-017-3580-6.

Cao, J., Ma, L., Liu, F., Chai, J., Zhao, H., He, Q., Wang, Bo, Bao, Y., Li, J., Yang, Y., Deng, H., Wang, Bin, 2021. NUIST ESM v3 Data Submission to CMIP6. Adv. Atmos. Sci. 38, 268–284. https://doi.org/10.1007/s00376-020-0173-9.

Carrier, M.-A., Lefebvre, R., Rivard, C., Parent, M., Ballard, J.-M., Benoit, N., Vigneault, H., Beaudry, C., Malet, X., Laurencelle, M., Gosselin, J.-S., Ladevèze, P., Thériault, R., Beaudin, I., Michaud, A., Pugin, A., Morin, R., Crow, H., Gloaguen, E., Bleser, J., Martin, A., Lavoie, D., 2013. Portrait des ressources en eau souterraine en Montérégie Est, Québec, Canada (No. INRS R-1433). Institut national de la recherche scientifique (INRS), Commission géologique du Canada (CGC), Organisme de bassin versant de la Yamaska (OBV Yamaska), Institut de recherche et développement en agroenvironnement (IRDA), Québec.

Cloutier, V., Blanchette, D., Dallaire, P.-L., Nadeau, S., Rosa, E., Roy, M., 2013. Projet d'acquisition de connaissances sur les eaux souterraines de l'Abitibi-Témiscamingue (partie 1) (No. P001). Groupe de recherche sur l'eau souterraine, Institut de recherche en mines et en environnement, Université du Québec en Abitibi-Témiscamingue, Québec.

Cloutier, V., Rosa, E., Nadeau, S., Dallaire, P.-L., Blanchette, D., Roy, M., 2015. Projet d'acquisition de connaissances sur les eaux souterraines de l'Abitibi-Témiscamingue (partie 2) (No. P002.R3). Groupe de recherche sur l'eau souterraine, Institut de recherche en mines et en environnement, Université du Québec en Abitibi-Témiscamingue, Québec.

Cochand, F., 2014. Impact des changements climatiques et du développement urbain sur les ressources en eaux du bassin versant de la rivière Saint-Charles.

Cochand, F., Therrien, R., Lemieux, J.-M., 2019. Integrated Hydrological Modeling of Climate Change Impacts in a Snow-Influenced Catchment. Groundwater 57, 3–20. https://doi.org/10.1111/gwat.12848.

Comeau, G., Talbot-Poulin, M.C., Tremblay, Y., Ayotte, S., Molson, J., Lemieux, J.M., Montcoudiol, N., Therrien, R., Fortier, R., Therrien, P., Fabien-Ouellet, G., 2013. Projet d'acquisition de connaissances sur les eaux souterraines en Outaouais. Département de géologie et de génie géologique, Université Laval, Québec.

Commission for Environmental Cooperation, 2020. 2015 Land Cover of North America ar 30 meters [WWW Document]. Commission for Environmental Cooperation. URL ⟨http://www.cec.org/north-american-environmental-atlas/land-cover-30m-2015-landsat-and-rapideye/⟩ (accessed 12.1.23).

Conrad, O., Bechtel, B., Bock, M., Dietrich, H., Fischer, E., Gerlitz, L., Wehberg, J., Wichmann, V., Böhner, J., 2015. System for Automated Geoscientific Analyses (SAGA) v. 2.1.4. Geosci. Model Dev. 8, 1991–2007. https://doi.org/10.5194/gmd-8-1991-2015.

Coron, L., Andréassian, V., Perrin, C., Bourqui, M., Hendrickx, F., 2014. On the lack of robustness of hydrologic models regarding water balance simulation: a diagnostic approach applied to three models of increasing complexity on 20 mountainous catchments. Hydrol. Earth Syst. Sci. 18, 727–746. https://doi.org/10.5194/hess-18-727-2014.

Dallaire, G., Poulin, A., Arsenault, R., Brissette, F., 2021. Uncertainty of potential evapotranspiration modelling in climate change impact studies on low flows in North America. Hydrol. Sci. J. 66, 689–702. https://doi.org/10.1080/02626667.2021.1888955.

Demil, G., Torabi Haghighi, A., Klöve, B., Oussalah, M., 2025. Advances in image-based estimation of snow variables: A systematic literature review on recent studies. J. Hydrol. 626, 132855. https://doi.org/10.1016/j.jhydrol.2025.132855.

Devia, G.K., Ganasri, B.P., Dwarakish, G.S., 2015. A Review on Hydrological Models. Aquatic Procedia, INTERNATIONAL CONFERENCE ON WATER RESOURCES, COASTAL AND OCEAN ENGINEERING (ICWRCOE'15) 4, 1001–1007. ⟨https://doi.org/10.1016/j.aqpro.2015.02.126⟩.

Dieng, A.S., Dieye, E.H.B., Diedhiou, A., 2022. Multivariate bias correction of climate projections over West Africa using MBCn. e2021JD034836 J. Geophys. Res.: Atmospheres 127. https://doi.org/10.1029/2021JD034836.

Döscher, R., Acosta, M., Alessandri, A., Anthoni, P., Arsouze, T., Bergman, T., Bernardello, R., Boussetta, S., Caron, L.-P., Carver, G., Castrillo, M., Catalano, F., Cvijanovic, I., Davini, P., Dekker, E., Doblas-Reyes, F.J., Docquier, D., Echevarria, P., Fladrich, U., Fuentes-Franco, R., Gröger, M., v. Hardenberg, J., Hieronymus, J., Karami, M.P., Keskinen, J.-P., Koenigk, T., Makkonen, R., Massonnet, F., Ménégoz, M., Miller, P.A., Moreno-Chamarro, E., Nieradzik, L., van Noije, T., Nolan, P., O'Donnell, D., Ollinaho, P., van den Oord, G., Ortega, P., Prims, O.T., Ramos, A., Reerink, T., Rousset, C., Ruprich-Robert, Y., Le Sager, P., Schmith, T., Schrödner, R., Serva, F., Sicardi, V., Sloth Madsen, M., Smith, B., Tian, T., Tourigny, E., Uotila, P., Vancoppenolle, M., Wang, S., Wårlind, D., Willén, U., Wyser, K., Yang, S., Yepes-Arbós, X., Zhang, Q., 2022. The EC-Earth3 Earth system model for the Coupled Model Intercomparison Project 6. Geosci. Model Dev. 15, 2973–3020. https://doi.org/10.5194/gmd-15-2973-2022.

Dubois, E., Larocque, M., Gagné, S., Braun, M., 2022. Climate Change Impacts on Groundwater Recharge in Cold and Humid Climates: Controlling Processes and Thresholds. Climate 10, 6. https://doi.org/10.3390/cli10010006.

Duethmann, D., Blöschl, G., Parajka, J., 2020. Why does a conceptual hydrological model fail to correctly predict discharge changes in response to climate change. Hydrol. Earth Syst. Sci. 24, 3493–3511. https://doi.org/10.5194/hess-24-3493-2020.

Ekmekcioğlu, Ö., Demirel, M.C., Booij, M.J., 2022. Effect of data length, spin-up period and spatial model resolution on fully distributed hydrological model calibration in the Moselle basin. Hydrol. Sci. J. 67, 759–772. https://doi.org/10.1080/02626667.2022.2046754.
Estrada, F., Kim, D., Perron, P., 2021. Spatial variations in the warming trend and the transition to more severe weather in midlatitudes. Sci. Rep. 11, 145. https://doi.org/10.1038/s41598-020-80701-7.
Gädeke, A., Hölzel, H., Koch, H., Pohle, I., Grünewald, U., 2014. Analysis of uncertainties in the hydrological response of a model-based climate change impact assessment in a subcatchment of the Spree River, Germany. Hydrol. Process. 28, 3978–3998. https://doi.org/10.1002/hyp.9933.
Gleick, P.H., 1989. Climate change, hydrology, and water resources. Rev. Geophys. 27, 329–344. https://doi.org/10.1029/rg027i003p00329.
Gombault, C., Sottile, M.-F., Ngwa, F.F., Madramootoo, C.A., Michaud, A.R., Beaudin, I., Chikhaoui, M., 2015. Modelling climate change impacts on the hydrology of an agricultural watershed in southern Québec. Can. Water Resour. J. / Rev. Can. Des. Ressour. Hydr. 40, 71–86. https://doi.org/10.1080/07011784.2014.985509.
Grinevskiy, S.O., Pozdniakov, S.P., Dedulina, E.A., 2021. Regional-Scale Model Analysis of Climate Changes Impact on the Water Budget of the Critical Zone and Groundwater Recharge in the European Part of Russia. Water 13, 428. https://doi.org/10.3390/w13040428.
Guo, D., Westra, S., Maier, H.R., 2020. An R package for performing multivariate bias correction of climate model output. e2019WR026659 Water Resour. Res. 56. https://doi.org/10.1029/2019WR026659.
Han, F., Zheng, Y., Tian, Y., Li, Xi, Zheng, C., Li, Xin, 2021. Accounting for field-scale heterogeneity in the ecohydrological modeling of large arid river basins: Strategies and relevance. J. Hydrol. 595, 126045. https://doi.org/10.1016/j.jhydrol.2021.126045.
Hausfather, Z., Marvel, K., Schmidt, G.A., Nielsen-Gammon, J.W., Zelinka, M., 2022. Climate simulations: recognize the "hot model" problem. Nature 605, 26–29. https://doi.org/10.1038/d41586-022-01192-2.
Hersbach, H., Bell, B., Berrisford, P., Hirahara, S., Horányi, A., Muñoz-Sabater, J., Nicolas, J., Peubey, C., Radu, R., Schepers, D., Simmons, A., Soci, C., Abdalla, S., Abellan, X., Balsamo, G., Bechtold, P., Biavati, G., Bidlot, J., Bonavita, M., De Chiara, G., Dahlgren, P., Dee, D., Diamantakis, M., Dragani, R., Flemming, J., Forbes, R., Fuentes, M., Geer, A., Haimberger, L., Healy, S., Hogan, R.J., Hólm, E., Janisková, M., Keeley, S., Laloyaux, P., Lopez, P., Lupu, C., Radnoti, G., de Rosnay, P., Rozum, I., Vamborg, F., Villaume, S., Thépaut, J.-N., 2020. The ERA5 global reanalysis. Q. J. R. Meteorol. Soc. 146, 1999–2049. https://doi.org/10.1002/qj.3803.
Houle, D., Bouffard, A., Duchesne, L., Logan, T., Harvey, R., 2012. Projections of Future Soil Temperature and Water Content for Three Southern Quebec Forested Sites. ⟨https://doi.org/10.1175/JCLI-D-11-00440.1⟩.
Hydroclimatic Atlas of Southern Québec [WWW Document], 2022. URL ⟨https://www.cehq.gouv.qc.ca/atlas-hydroclimatique/index-en.htm⟩ (accessed 11.30.23).
Iacob, O., Brown, I., Rowan, J., 2017. Natural flood management, land use and climate change trade-offs: the case of Tarland catchment, Scotland. Hydrol. Sci. J. 62, 1931–1948. https://doi.org/10.1080/02626667.2017.1366657.
Jasper, K., Calanca, P., Fuhrer, J., 2006. Changes in summertime soil water patterns in complex terrain due to climatic change. J. Hydrol. 327, 550–563. https://doi.org/10.1016/j.jhydrol.2005.11.061.
Jones, R.N., Chiew, F.H.S., Boughton, W.C., Zhang, L., 2006. Estimating the sensitivity of mean annual runoff to climate change using selected hydrological models. Adv. Water Resour. 29, 1419–1429. https://doi.org/10.1016/j.advwatres.2005.11.001.
Kling, H., Fuchs, M., Paulin, M., 2012. Runoff conditions in the upper Danube basin under an ensemble of climate change scenarios. J. Hydrol. 424–425, 264–277. https://doi.org/10.1016/j.jhydrol.2012.01.011.
Kour, R., Patel, N., Krishna, A.P., 2016. Climate and hydrological models to assess the impact of climate change on hydrological regime: a review. Arab J. Geosci. 9, 544. https://doi.org/10.1007/s12517-016-2561-0.
Krasting, J.P., Blanton, C., McHugh, C., Radhakrishnan, A., John, J.G., Rand, K., Nikonov, S., Vahlenkamp, H., Zadeh, N.T., Dunne, J.P., Shevliakova, E., Horowitz, L. W., Stock, C., Malyshev, S., Ploshay, J., Gauthier, P.P., Naik, V., Winton, M., Zeng, Y., 2018. NOAA-GFDL GFDL-ESM4 model output prepared for CMIP6 C4MIP esm-ssp585.
Larocque, M., Gagné, S., Barnetche, D., Meyzonnat, G., Graveline, M.-H., Ouellet, M.A., 2015. Projet de connaissance des eaux souterraines du bassin versant de la zone Nicolet et de la partie basse de la zone Saint-François - Rapport final. Ministère du Développement durable, de l'Environnement et de la Lutte contre les changements climatiques, Québec.
Larocque, M., Gagné, S., Tremblay, L., Meyzonnat, G., 2013. Projet de connaissance des eaux souterraines du bassin versant de la rivière Bécancour et de la MRC de Bécancour - Rapport final. Ministère du Développement durable, de l'Environnement, de la Faune et des Parcs, Québec.
Latifovic, R., Homer, C., Ressl, R., Pouliot, D.A., Hossian, S., Colditz, R., Olthof, I., Chandra, G., Victoria, A., 2012. North American Land Change Monitoring System. Remote Sensing of Land Use and Land Cover: Principles and Applications 303–324. ⟨https://doi.org/10.1201/b11964-24⟩.
Lefebvre, R., Ballard, J.-M., Vigneault, H., Beaudry, C., Berthot, L., Légaré-Couture, G., Parent, M., Laurencelle, M., Malet, X., Therrien, A., Michaud, A., Desjardins, J., Drouin, A., Cloutier, M.H., Grenier, J., Bourgault, M.-A., Larocque, M., Pellerin, S., Graveline, M.-H., Janos, D., Molson, J., 2015. Portrait des ressources en eau souterraine en Chaudière-Appalaches, Québec, Canada (No. INRS R-1580). Institut national de la recherche scientifique (INRS), Institut de recherche et développement en agroenvironnement (IRDA), Regroupement des organismes de bassins versants de la Chaudière-Appalaches (OBV-CA), Québec.
Lindquist, L.W., Palmquist, K.A., Jordan, S.E., Lauenroth, W.K., 2019. Impacts of Climate Change on Groundwater Recharge in Wyoming Big Sagebrush Ecosystems are Contingent on Elevation. wnan 79, 37–48. https://doi.org/10.3398/064.079.0104.
Lovato, T., Peano, D., Butenschön, M., Materia, S., Iovino, D., Scoccimarro, E., Fogli, P.G., Cherchi, A., Bellucci, A., Gualdi, S., Masina, S., Navarra, A., 2022. CMIP6 Simulations With the CMCC Earth System Model (CMCC-ESM2). e2021MS002814 J. Adv. Model. Earth Syst. 14. https://doi.org/10.1029/2021MS002814.
Lucas-Picher, P., Lachance-Cloutier, S., Arsenault, R., Poulin, A., Ricard, S., Turcotte, R., Brissette, F., 2021. Will Evolving Climate Conditions Increase the Risk of Floods of the Large U.S.-Canada Transboundary Richelieu River Basin? JAWRA J. Am. Water Resour. Assoc. 57, 32–56. https://doi.org/10.1111/1752-1688.12891.
Ludwig, R., May, I., Turcotte, R., Vescovi, L., Braun, M., Cyr, J.-F., Fortin, L.-G., Chaumont, D., Biner, S., Chartier, I., Caya, D., Mauser, W., 2009. The role of hydrological model complexity and uncertainty in climate change impact assessment. Adv. Geosci. 21, 63–71. https://doi.org/10.5194/adgeo-21-63-2009.
Lundberg, A., Ala-Aho, P., Eklo, O., Klöve, B., Kværner, J., Stumpp, C., 2016. Snow and frost: implications for spatiotemporal infiltration patterns – a review. Hydrol. Process. 30, 1230–1250. https://doi.org/10.1002/hyp.10703.
Martel, J.-L., Brissette, F., Troin, M., Arsenault, R., Chen, J., Su, T., Lucas-Picher, P., 2022. CMIP5 and CMIP6 Model Projection Comparison for Hydrological Impacts Over North America. e2022GL098364 Geophys. Res. Lett. 49. https://doi.org/10.1029/2022GL098364.
Mauritsen, T., Bader, J., Becker, T., Behrens, J., Bittner, M., Brokopf, R., Brovkin, V., Claussen, M., Crueger, T., Esch, M., Fast, I., Fiedler, S., Fläschner, D., Gayler, V., Giorgetta, M., Goll, D.S., Haak, H., Hagemann, S., Hedemann, C., Hohenegger, C., Ilyina, T., Jahns, T., Jimenéz-de-la-Cuesta, D., Jungclaus, J., Kleinen, T., Kloster, S., Kracher, D., Kinne, S., Kleberg, D., Lasslop, G., Kornblueh, L., Marotzke, J., Matei, D., Meraner, K., Mikolajewicz, U., Modali, K., Möbis, B., Müller, W. A., Nabel, J.E.M.S., Nam, C.C.W., Notz, D., Nyawira, S.-S., Paulsen, H., Peters, K., Pincus, R., Pohlmann, H., Pongratz, J., Popp, M., Raddatz, T.J., Rast, S., Redler, R., Reick, C.H., Rohrschneider, T., Schemann, V., Schmidt, H., Schnur, R., Schulzweida, U., Six, K.D., Stein, L., Stemmler, I., Stevens, B., von Storch, J.-S., Tian, F., Voigt, A., Vrese, P., Wieners, K.-H., Wilkenskjeld, S., Winkler, A., Roeckner, E., 2019. Developments in the MPI-M Earth System Model version 1.2 (MPI-ESM1.2) and Its Response to Increasing CO2. J. Adv. Model. Earth Syst. 11, 998–1038. https://doi.org/10.1029/2018MS001400.
McDonnell, J.J., Spence, C., Karran, D.J., van Meerveld, H.J., (Ilja), Harman, C.J., 2021. Fill-and-Spill: A Process Description of Runoff Generation at the Scale of the Beholder. e2020WR027514 Water Resour. Res. 57. https://doi.org/10.1029/2020WR027514.
Meert, P., Pereira, F., Willems, P., 2018. Surrogate modeling-based calibration of hydrodynamic river model parameters. J. Hydrol. Eng. Res. 4 (1), 1–12. https://doi.org/10.1016/j.jher.2018.02.003.
Middelkoop, H., Daamen, K., Gellens, D., Grabs, W., Kwadijk, J.C.J., Lang, H., Parmet, B.W.A.H., Schädler, B., Schulla, J., Wilke, K., 2001. Impact of Climate Change on Hydrological Regimes and Water Resources Management in the Rhine Basin. Clim. Change 49, 105–128. https://doi.org/10.1023/A:1010784727448.
Milly, P.C.D., Betancourt, J., Falkenmark, M., Hirsch, R.M., Kundzewicz, Z.W., Lettenmaier, D.P., Stouffer, R.J., 2008. Stationarity Is Dead: Whither Water Management. Science 319, 573–574. https://doi.org/10.1126/science.1151915.

Milly, P.C.D., Dunne, K.A., Vecchia, A.V., 2005. Global pattern of trends in streamflow and water availability in a changing climate. Nature 438, 347–350. https://doi.org/10.1038/nature04312.
Ministère des Ressources Naturelles et des Forêts, 2022. SIIGSOL-100m - Carte des propriétés du sol. Données Québec. Updated June 26, 2023. ⟨https://www.donneesquebec.ca/recherche/dataset/siigsol-100m-carte-des-proprietes-du-sol⟩ (accessed May 1, 2025).
Minville, M., Brissette, F., Leconte, R., 2008. Uncertainty of the impact of climate change on the hydrology of a nordic watershed. J. Hydrol. 358, 70–83. https://doi.org/10.1016/j.jhydrol.2008.05.033.
Mudryk, L.R., Derksen, C., Howell, S., Laliberté, F., Thackeray, C., Sospedra-Alfonso, R., Vionnet, V., Kushner, P.J., Brown, R., 2018. Canadian snow and sea ice: historical trends and projections. Cryosphere 12, 1157–1176. https://doi.org/10.5194/tc-12-1157-2018.
Natural Resources Canada, 2023. Evapotranspiration and evaporation in Canada [WWW Document]. URL ⟨https://geo.ca/fr/imagerie/evapotranspiration-et-evaporation-au-canada⟩ (accessed 07.17.24).
Nolin, A.F., Girardin, M.P., Adamowski, J.F., Barzegar, R., Boucher, M.-A., Tardif, J.C., Bergeron, Y., 2023. Observed and projected trends in spring flood discharges for the Upper Harricana River, eastern boreal Canada. J. Hydrol.: Reg. Stud. 48, 101462. https://doi.org/10.1016/j.ejrh.2023.101462.
Novotná, B., van Bochove, E., Thériault, G., 2013. Potential ecological impact of climate change on the water quality of an intensively managed agricultural watershed in Quebec, Canada. J. Water Clim. Change 5, 81–99. https://doi.org/10.2166/wcc.2013.121.
O'Neill, B.C., Tebaldi, C., van Vuuren, D.P., Eyring, V., Friedlingstein, P., Hurtt, G., Knutti, R., Kriegler, E., Lamarque, J.-F., Lowe, J., Meehl, G.A., Moss, R., Riahi, K., Sanderson, B.M., 2016. The Scenario Model Intercomparison Project (ScenarioMIP) for CMIP6. Geosci. Model Dev. 9, 3461–3482. https://doi.org/10.5194/gmd-9-3461-2016.
Poulin, A., Brissette, F., Leconte, R., Arsenault, R., Malo, J.-S., 2011. Uncertainty of hydrological modelling in climate change impact studies in a Canadian, snow-dominated river basin. J. Hydrol. 409, 626–636. https://doi.org/10.1016/j.jhydrol.2011.08.057.
Pu, Y., Liu, H., Yan, R., Yang, H., Xia, K., Li, Y., Dong, L., Li, L., Wang, H., Nie, Y., Song, M., Xie, J., Zhao, S., Chen, K., Wang, B., Li, J., Zuo, L., 2020. CAS FGOALS-g3 Model Datasets for the CMIP6 Scenario Model Intercomparison Project (ScenarioMIP. Adv. Atmos. Sci. 37, 1081–1092. https://doi.org/10.1007/s00376-020-2032-0.
Riboust, P., Brissette, F., 2015. Climate Change Impacts and Uncertainties on Spring Flooding of Lake Champlain and the Richelieu River. JAWRA J. Am. Water Resour. Assoc. 51, 776–793. https://doi.org/10.1111/jawr.12271.
Ricard, S., Sylvain, J.-D., Anctil, F., 2019. Exploring an Alternative Configuration of the Hydroclimatic Modeling Chain, Based on the Notion of Asynchronous Objective Functions. Water 11, 2012. https://doi.org/10.3390/w11102012.
Ricard, S., Sylvain, J.-D., Anctil, F., 2020. Asynchronous Hydroclimatic Modeling for the Construction of Physically Based Streamflow Projections in a Context of Observation Scarcity. Front. Earth Sci. 8.
Richards, L.A., 1931. Capillary conduction of liquids through porous mediums. Physics 1 (5), 318–333. https://doi.org/10.1063/1.1745010.
Rouleau, A., Daigneault, R., Walter, J., Germaneau, D., Tremblay, M.-L., Lambert, M., Dallaire, C., Chesnaux, R., Cousineau, P.A., Roy, D.W., Noël, D., Simard, P., Moisan, A., Thouvignon, N., 2013. Résultats du programme d'acquisition de connaissances sur les eaux souterraines de la région Saguenay-Lac-Saint-Jean. Centre d'études sur les ressources minérales, Université du Québec à Chicoutimi, Chicoutimi, Québec.
Schulla, J., 2021. WaSiM-ETH Documentation [WWW Document]. URL ⟨http://www.wasim.ch/en/products/wasim_description.htm⟩ (accessed 11.30.23).
Seland, Ø., Bentsen, M., Olivié, D., Toniazzo, T., Gjermundsen, A., Graff, L.S., Debernard, J.B., Gupta, A.K., He, Y.-C., Kirkevåg, A., Schwinger, J., Tjiputra, J., Aas, K. S., Bethke, I., Fan, Y., Griesfeller, J., Grini, A., Guo, C., Ilicak, M., Karset, I.H.H., Landgren, O., Liakka, J., Moseid, K.O., Nummelin, A., Spensberger, C., Tang, H., Zhang, Z., Heinze, C., Iversen, T., Schulz, M., 2020. Overview of the Norwegian Earth System Model (NorESM2) and key climate response of CMIP6 DECK, historical, and scenario simulations. Geosci. Model Dev. 13, 6165–6200. https://doi.org/10.5194/gmd-13-6165-2020.
Sivakumar, B., 2011. Global climate change and its impacts on water resources planning and management: assessment and challenges. Stoch. Environ. Res Risk Assess. 25, 583–600. https://doi.org/10.1007/s00477-010-0423-y.
Sulis, M., Paniconi, C., Rivard, C., Harvey, R., Chaumont, D., 2011. Assessment of climate change impacts at the catchment scale with a detailed hydrological model of surface-subsurface interactions and comparison with a land surface model. Water Resour. Res. 47. https://doi.org/10.1029/2010WR009167.
Swart, N.C., Cole, J.N.S., Kharin, V.V., Lazare, M., Scinocca, J.F., Gillett, N.P., Anstey, J., Arora, V., Christian, J.R., Hanna, S., Jiao, Y., Lee, W.G., Majaess, F., Saenko, O.A., Seiler, C., Seinen, C., Shao, A., Sigmond, M., Solheim, L., von Salzen, K., Yang, D., Winter, B., 2019. The Canadian Earth System Model version 5 (CanESM5.0.3). Geosci. Model Dev. 12, 4823–4873. https://doi.org/10.5194/gmd-12-4823-2019.
Sylvain, J.-D., Anctil, F., Thiffault, E., 2021. Using bias correction and ensemble modelling for predictive mapping and related uncertainty: A case study in digital soil mapping. Geoderma 403, 1–29. https://doi.org/10.1016/j.geoderma.2021.115153.
Talbot, F., Sylvain, J.-D., Drolet, G., Poulin, A., Arsenault, R., 2024a. Enhancing physically based and distributed hydrological model calibration through internal state variable constraints. EGUsphere. https://doi.org/10.5194/egusphere-2024-3353 [preprint].
Talbot, F., Sylvain, J.-D., Drolet, G., Poulin, A., Arsenault, R., 2024b. Journal of Hydrology paper data - Wasim climate change impacts on hydrology. ⟨https://doi.org/10.17605/OSF.IO/D9WZE⟩.
Tarek, M., Brissette, F.P., Arsenault, R., 2020. Evaluation of the ERA5 reanalysis as a potential reference dataset for hydrological modelling over North America. Hydrol. Earth Syst. Sci. 24, 2527–2544. https://doi.org/10.5194/hess-24-2527-2020.
Tarek, M., Brissette, F., Arsenault, R., 2021. Uncertainty of gridded precipitation and temperature reference datasets in climate change impact studies. Hydrol. Earth Syst. Sci. 25, 3331–3350. https://doi.org/10.5194/hess-25-3331-2021.
Tatebe, H., Ogura, T., Nitta, T., Komuro, Y., Ogochi, K., Takemura, T., Sudo, K., Sekiguchi, M., Abe, M., Saito, F., Chikira, M., Watanabe, S., Mori, M., Hirota, N., Kawatani, Y., Mochizuki, T., Yoshimura, K., Takata, K., O'ishi, R., Yamazaki, D., Suzuki, T., Kurogi, M., Kataoka, T., Watanabe, M., Kimoto, M., 2019. Description and basic evaluation of simulated mean state, internal variability, and climate sensitivity in MIROC6. Geosci. Model Dev. 12, 2727–2765. https://doi.org/10.5194/gmd-12-2727-2019.
Taylor, K.E., Stouffer, R.J., Meehl, G.A., 2012. An Overview of CMIP5 and the Experiment Design. Bull. Am. Meteorol. Soc. 93, 485–498. https://doi.org/10.1175/BAMS-D-11-00094.1.
Tolson, B.A., Shoemaker, C.A., 2007. Dynamically dimensioned search algorithm for computationally efficient watershed model calibration. Water Resour. Res. 43, W01413. https://doi.org/10.1029/2005WR004723.
Valencia Giraldo, M., del, C., Ricard, S., Anctil, F., 2023. Assessment of the Potential Hydrological Impacts of Climate Change in Quebec—Canada, a Refined Neutral Approach. Water 15, 584. https://doi.org/10.3390/w15030584.
Volodin, E., Mortikov, E., Gritsun, A., Lykossov, V., Galin, V., Diansky, N., Gusev, A., Kostrykin, S., Iakovlev, N., Shestakova, A., Emelina, S., 2019. INM INM-CM4-8 model output prepared for CMIP6 CMIP.
Weil, R., Brady, N., 2017. The Nature and Properties of Soils. 15th edition.
Wilby, R.L., 2005. Uncertainty in water resource model parameters used for climate change impact assessment. Hydrol. Process. 19, 3201–3219. https://doi.org/10.1002/hyp.5819.
Wright, S.N., Novakowski, K.S., 2020. Impacts of warming winters on recharge in a seasonally frozen bedrock aquifer. J. Hydrol. 590, 125352. https://doi.org/10.1016/j.jhydrol.2020.125352.
Yue, X.-L., Gao, Q.-X., 2018. Contributions of natural systems and human activity to greenhouse gas emissions. Adv. Clim. Change Res. 9, 243–252. https://doi.org/10.1016/j.accre.2018.12.003.
Yukimoto, S., Kawai, H., Koshiro, T., Oshima, N., Yoshida, K., Urakawa, S., Tsujino, H., Deushi, M., Tanaka, T., Hosaka, M., Yabu, S., Yoshimura, H., Shindo, E., Mizuta, R., Obata, A., Adachi, Y., Ishii, M., 2019. The Meteorological Research Institute Earth System Model Version 2.0. MRI-ESM2. 0: Descr. Basic Eval. Phys. Compon. 気象集誌. 第2輯 97, 931–965. https://doi.org/10.2151/jmsj.2019-051.
Ziehn, T., Chamberlain, M.A., Law, R.M., Lenton, A., Bodman, R.W., Dix, M., Stevens, L., Wang, Y.-P., Srbinovsky, J., 2020. The Australian Earth System Model: ACCESS-ESM1.5. JSHESS 70, 193–214. https://doi.org/10.1071/ES19035.